

ORIGINAL RESEARCH

Inward Rectifier K⁺ Currents Contribute to the Proarrhythmic Electrical Phenotype of Atria Overexpressing Cyclic Adenosine Monophosphate Response Element Modulator Isoform CREM-IbΔC-X

Florentina Pluteanu , PhD*; Matthias D. Seidl, PhD*; Sabine Hamer, PhD; Beatrix Scholz, PhD; Frank U. Müller, MD

BACKGROUND: Transgenic mice (TG) with heart-directed overexpression of the isoform of the transcription factor cyclic adenosine monophosphate response element modulator (CREM), CREM-IbΔC-X, display spontaneous atrial fibrillation (AF) and action potential prolongation. The remodeling of the underlying ionic currents remains unknown. Here, we investigated the regulatory role of CREM-IbΔC-X on the expression of K⁺ channel subunits and the corresponding K⁺ currents in relation to AF onset in TG atrial myocytes.

METHODS AND RESULTS: ECG recordings documented the absence or presence of AF in 6-week-old (before AF onset) and 12-week-old TG (after AF onset) and wild-type littermate mice before atria removal to perform patch clamp, contractility, and biochemical experiments. In TG atrial myocytes, we found reduced repolarization reserve K⁺ currents attributed to a decrease of transiently outward current and inward rectifier K⁺ current with phenotype progression, and of acetylcholine-activated K⁺ current, age independent. The molecular determinants of these changes were lower mRNA levels of *Kcnd2/3*, *Kcnp2*, *Kcnj2/4*, and *Kcnj3/5* and decreased protein levels of K⁺ channel interacting protein 2 (KChIP2), Kir2.1/3, and Kir3.1/4, respectively. After AF onset, inward rectifier K⁺ current contributed less to action potential repolarization, in line with the absence of outward current component, whereas the acetylcholine-induced action potential shortening before AF onset (6-week-old TG mice) was smaller than in wild-type and 12-week-old TG mice. Atrial force of contraction measured under combined vagal-sympathetic stimulation revealed increased sensitivity to isoprenaline irrespective of AF onset in TG. Moreover, we identified *Kcnd2*, *Kcnd3*, *Kcnj3*, and *Kcnh2* as novel CREM-target genes.

CONCLUSIONS: Our study links the activation of cyclic adenosine monophosphate response element-mediated transcription to the proarrhythmogenic electrical remodeling of atrial inward rectifier K⁺ currents with a role in action potential duration, resting membrane stability, and vagal control of the electrical activity.

Key Words: atrial fibrillation ■ electrical remodeling ■ inward rectifiers ■ K⁺ channel

Patients manifesting atrial fibrillation (AF) present a variety of altered molecular mechanisms.¹ Therapeutically, identifying the functional alterations in the early stages of the disease would be

beneficial. In this regard, animal models of AF are useful tools to identify AF onset time and to investigate biological alterations occurring early in atrial remodeling. Experimental AF were induced either functionally

Correspondence to: Florentina Pluteanu, Institut für Pharmakologie und Toxikologie, Westfälische Wilhelms-Universität Münster, Domagkstr. 12, D-48149 Münster, Germany. E-mail: fpluteanu@gmail.com

Supplementary Material for this article is available at <https://www.ahajournals.org/doi/suppl/10.1161/JAHA.119.016144>

*Dr Pluteanu and Dr Seidl contributed equally to this work.

For Sources of Funding and Disclosures, see page 17.

© 2020 The Authors. Published on behalf of the American Heart Association, Inc., by Wiley. This is an open access article under the terms of the Creative Commons Attribution-NonCommercial-NoDerivs License, which permits use and distribution in any medium, provided the original work is properly cited, the use is non-commercial and no modifications or adaptations are made.

JAHA is available at: www.ahajournals.org/journal/jaha

CLINICAL PERSPECTIVE

What Is New?

- This study identified a complex electrical remodeling in atrial myocytes from cyclic adenosine monophosphate response element modulator isoform CREM-IbΔC-X transgenic mice, consisting of the downregulation of many K⁺ channel subunits linked to familial forms of long QT syndrome as well as of the corresponding K⁺ currents, which contribute to action potential prolongation, atrial fibrillation, and autonomic cardiac dysregulation.
- We showed that genes encoding these K⁺ channels are targeted by the transcriptional repressor CREM isoform CREM-IbΔC-X.
- Our study supports the multifactorial causes of atrial fibrillation and suggests that overlapped decrease of the transiently outward current, inward rectifier K⁺ current, and acetylcholine-activated K⁺ current and increased sensitivity to sympathetic stimulation creates an electrical substrate for atrial fibrillation development and maintenance.

What Are the Clinical Implications?

- This study identified new cardiomyocyte-specific proarrhythmogenic mechanisms modulated by cyclic adenosine monophosphate-activated transcription factors such as CREM.
- Our study proposes a direct link between the expression of CREM isoforms and atrial failure-associated electrical remodeling.
- Discovery of new drugs that modulate molecular targets such as ion channels or the activity of transcription factors with roles in electrical stability at the cardiomyocyte level may be beneficial for future therapeutic strategies to control arrhythmias in the treatment of patients with atrial fibrillation.

Nonstandard Abbreviations and Acronyms

AM	atrial myocytes
AP	action potential
APD	action potential duration
ATF1	activating transcription factor 1
ChIP	chromatin immunoprecipitation
CREB	cyclic adenosine monophosphate response element binding protein
CREM	cyclic adenosine monophosphate response element modulator
ETV1	E twenty-six variant 1

FKBP12	FK506-binding protein 12
FOC	force of contraction
GIRK	G-protein coupled inwardly rectifying K ⁺ channel
I_{K1}	inward rectifier K ⁺ current
I_{KACH}	acetylcholine-activated K ⁺ current
I_{Kend}	total outward K ⁺ current at the end of the pulse
I_{Kr}	cardiac “rapid” delayed rectifier current
I_{Ks}	slow-activating slow-inactivating delayed rectifier K ⁺ current
I_{Ktail}	tail K ⁺ current
I_{to}	transiently outward current
KChIP2	K ⁺ channel interacting protein 2
KCNE2	K ⁺ voltage-gated channel subfamily E regulatory subunit 2
M₂R	muscarinic M ₂ -receptor
FKBP12	FK506-binding protein 12
qRT-PCR	quantitative real-time polymerase chain reaction
RMP	resting membrane potential
TBX5	T-box transcription factor 5
TG	transgenic mice expressing CREM-IbΔC-X transcription factor
WT	wild type
βAR	β-adrenoceptor

in large animals by rapid atrial pacing^{2–5} or by genetic modifications of a variety of molecules ranging from (1) ion channels such as Nav1.5,⁶ (2) adaptor proteins such as FK506-binding protein (FKBP12),⁷ or (3) transcription factors such as E twenty-six variant 1 (ETV1),⁸ T-box transcription factor (TBX5),⁹ paired-like homeodomain 2 (PITX2),¹⁰ or cyclic adenosine monophosphate (cAMP) response element modulator (CREM).¹¹ These AF animal models showed similarities with human AF and allow the identification of pathophysiological mechanisms linked to a specific alteration.

CREM-IbΔC-X is an isoform of the CREM transcription factor that functions as a repressor of cAMP signaling-induced transcription belonging to the cAMP response element binding (CREB) and activating transcription factor (ATF1) family.¹² Elevated levels of CREM-IbΔC-X were reported in patients with heart failure¹² and AF.¹³ The downregulation of target genes of CREB/ATF1 family of transcription factors was associated with AF susceptibility in humans.¹⁴ In mice, heart-directed overexpression of CREM-IbΔC-X induced extensive remodeling at structural and functional levels leading to an onset of atrial ectopic activity around 7 to 8 weeks of age that progressed to permanent AF by 12 weeks of age.^{15,16} The progression of

AF-induced remodeling in transgenic mice expressing CREM-IbΔC-X transcription factor (TG) recapitulates many aspects of the structural changes occurring before AF in patients,^{11,15} except for the changes of action potential duration (APD). Although AP shortening is considered the hallmark of AF, the atrial APD prolongation has been frequently reported in many mouse models for AF^{6,8,16,17} as well as for some patients with long QT syndrome.¹⁸

Characterization of the transcriptional program linked to AF development in these mice identified a switch from structural to functional remodeling from young to old mice,¹⁶ partially reversed by the anticonvulsant valproate.¹⁹ In TG, AF occurs in the absence of detrimental structural and hemodynamic ventricular remodeling¹¹ and in the presence of atrial dilation and prolonged APD.^{15,16} Reports from both heterozygous¹⁶ and homozygous TG mice²⁰ identified decreased mRNA levels of some genes encoding for K⁺ channel subunits. So far, any characterization of the ionic currents underlying the atrial AP prolongation in TG mice was not performed. Thus, we aimed to evaluate the changes in the electrophysiological profile of atrial myocytes (AM) isolated from TG mice in relation to AF onset.

METHODS

The data that support the findings of this study are available from the corresponding author upon reasonable request.

An expanded version of the methods is presented in Data S1.

Experimental Animals

Mice with cardiomyocyte-directed overexpression of hemagglutinin-tagged CREM-IbΔC-X (TG) were described previously.^{11,12} Wild-type (WT) littermates were used as control. Mice were kept at a room temperature of 22°C under a 12-hour light/dark cycle and received a normal diet (Altromin Spezialfutter GmbH, Lage, Germany) and water ad libitum. The mice were euthanized by CO₂ inhalation. Animals were handled and maintained according to the local welfare authority's rules and Directive 2010/63/EU of the European Parliament. All followed procedures were approved by and were in accordance with the institutional guidelines established by the regional authority Landesamt für Natur, Umwelt and Verbraucherschutz, North Rhine-Westphalia, Germany. The animals were distributed according to age (5–7 and 11–13 weeks) and genotype (WT and TG) into 4 groups: WT 6 weeks (WT_{6w}), TG 6 weeks (TG_{6w}), WT 12 weeks (WT_{12w}), and TG 12 weeks (TG_{12w}).

In Vivo ECG Measurements

ECG measurements were performed in isoflurane-anesthetized mice to confirm the absence (in WT_{6w}, TG_{6w}, and WT_{12w} mice) and the presence of persistent AF (in TG_{12w}). ECG measurements confirmed the presence of AF before heart removal for AM isolation for standard patch-clamp or atrial tissue homogenization for standard biochemical assays such as Western blot, quantitative real-time polymerase chain reaction (qRT-PCR), and chromatin immunoprecipitation (ChIP) as previously described.^{16,19} The number of TG mice exhibiting persistent AF at the age of 5 to 7 weeks was low and randomly detected to create an individual group. Moreover, this finding agreed with our aim, and therefore the mice not included in our study did not confound the experiment. It was essential to perform ECG measurements on all mice to test for AF presence or absence and to assign the animals to the proper group for the equal distribution of the samples; therefore, not all of the experimenters were blinded. Moreover, because of the strong atrial phenotype, the quality of cell isolation was poor in the TG mice, meaning that more TG than WT mice had to be euthanized for this study.

Tissue Isolation

Hearts were excised and transferred to ice-cold calcium-free Tyrode's solution. Both atria were quickly cut from the heart, frozen in liquid nitrogen, and stored for further analysis using qRT-PCR, Western blot, and ChIP assays.

Isolation of Atrial Cardiomyocytes

Atrial cardiomyocytes were isolated from all 4 groups of mice using retrograde perfusion of the hearts to digest the connective tissue with collagenase type II (230U/mg; Worthington Biochemical Corporation, Lakewood, NJ) as described previously.¹⁶

Electrophysiology

Ca²⁺-tolerant AM were used for the measurements of K⁺ currents using the patch-clamp technique in perforated-patch configuration achieved with the help of amphotericin B (300 µg/mL; Sigma-Aldrich Chemie GmbH, Steinheim, Germany). All recordings were performed at room temperature (22°C–24°C). Borosilicate glass capillaries (Science Products GmbH, Hofheim, Germany) were pulled to a resistance of 3 to 5 MΩ with a horizontal puller (P-97; Sutter Instruments Inc., Novato, CA). Data were sampled with an 18-bit analog to digital converter InstruTech ITC-18 and filtered at 10 kHz using an EPC-800 amplifier under the control of the PatchMaster software (HEKA Elektronik, Lambrecht, Germany). The

average values for the seal resistances was on average higher than 1 GΩ and not significantly different between groups. The series resistances reached on average between 22 and 24 MΩ and were compensated between 52% and 65%. To record the action potentials (AP) and K⁺ currents, the cells were perfused with a bath solution containing the following (in mmol/L): 136 NaCl, 5.4 KCl, 1 CaCl₂, 1 MgCl₂, 5 HEPES, 0.33 NaH₂PO₄, and 10 glucose adjusted to pH 7.4 with NaOH. The pipettes were filled with a solution containing the following (in mmol/L): 5 NaCl, 120 KCl, 2.5 MgATP, 1 EGTA, and 5 HEPES adjusted to pH 7.2 with KOH. The 10 μmol/L solution of BaCl₂ or acetylcholine were freshly prepared from 100 mmol/L BaCl₂ or 100 mmol/L acetylcholine stock solutions in water. The protocols used for recording the total outward K⁺ currents are described in Data S1. Briefly, voltage pulses in 10 mV increments from -80 mV or -40 mV to +70 mV were delivered from a holding voltage of -80 mV followed by a prepulse to -40 mV of either 10 milliseconds (to inactivate the sodium channel) or of 180 milliseconds (to inactivate the transient outward K⁺ channel). In the first protocol, the depolarizing steps were followed by a 300 milliseconds pulse to -120 mV for assessing the inward tail currents flowing through the delayed rectifier channels, to estimate indirectly the cardiac "rapid" delayed rectifier current (*I_{Kr}*) passing through human ether-a-go-go related gene channel (hERG). The inward rectifier K⁺ current was measured as the current at the end of the 500 milliseconds pulses between -120 and -10 mV from a -40 mV holding voltage. To assess the BaCl₂ and acetylcholine sensitive currents, a ramp protocol of 1-second duration between -120 to +60 mV from the holding voltage of -40 mV was applied at 30-second intervals. Current amplitudes (expressed in picoamperes [pA]) were measured as described in the supplemental data and were normalized to membrane capacitance (expressed in picofarads [pF]) of the cell to obtain the current density (pA/pF). AP were triggered at 1 Hz frequency with a suprathreshold current stimulus of 600 to 1000 pA amplitude and a 3-millisecond to 6-millisecond duration. Three to 5 consecutive AP traces at steady state were averaged, and AP amplitude, slope, and durations were measured from the peak to 20%, 50%, 70%, and 90% repolarizations using a macro for APD analysis designed by Dr Jan S. Schulte²¹ (University of Münster, Germany) for Origin 8.1 (OriginLab Corporation, Northampton, MA).

Western Blot

Atria from 6 to 8 mice were used from each group. Both the left and right atria were pooled from each

mouse and homogenized in lysis buffer containing 100 mmol/L NaCl, 20 mmol/L Tris base, 1% sodium deoxycholate, 0.1% SDS, 1% Triton X-100, and pH 8.0 and supplemented with phosphatase and protease inhibitor tablets (A32959; Thermo Fischer Scientific, Darmstadt, Germany). Protein concentration of the homogenates were measured using the classical Bradford method (Thermo Fisher Scientific). The samples were equally distributed, and 40 μg of protein homogenates was loaded per well on the 10% SDS-PAGE gel. Equal protein load was assessed after transfer using Ponceau stain. The following rabbit polyclonal primary antibodies were used against K⁺ voltage-gated channels (Kv) subunits Kv4.2 (1:200, APC 023, Alomone Labs, Jerusalem, Israel), Kv4.3 (1:200, APC 017, Alomone Labs), K⁺ channel interacting protein 2 (KChIP2) (1:200, sc-25685, Santa Cruz Biotechnology Inc, Santa Cruz, CA), and K⁺ inwardly rectifying channel (Kir) subunits Kir2.1 (1:200, APC 159, Alomone Labs), Kir2.3 (1:1000, APC 032, Alomone Labs), Kir3.1 (1:200, APC 005, Alomone Labs), Kir3.4 (1:200, APC 027, Alomone Labs), and as loading control calsequestrin (1:2500, PA1-913, Thermo Fisher Scientific). As secondary antibodies we used horseradish peroxidase conjugated anti-rabbit IgG antibody (1:10 000, A27036, Thermo Fisher Scientific). Chemiluminescence was developed with SERVALight Helios (42587.03, SERVA Electrophoresis GmbH, Heidelberg, Germany) or SERVALight Eos (42585.02, SERVA Electrophoresis GmbH). After developing the secondary antibody, the band intensity was quantified using ImageJ 1.49v (National Institute of Health, Bethesda, MD). Each band was normalized for load (to the Ponceau stain intensity of the full lane), for transfer (normalized to the averaged signal of the WT_{6w} bands of the same membrane, as reference), and to calsequestrin for myocyte content. The normalized values of the samples belonging to the same group were averaged for statistical comparison.

Quantitative Real-Time Polymerase Chain Reaction

A total of 8 animals have been used from each group. Total RNA was purified using TRIzol (15596018, Thermo Fisher Scientific) according to the manufacturer instructions, and 1 μg was reversely transcribed to cDNA that served as input for qRT-PCR. The primers used to probe the ion channel subunits are described in Data S1. Hypoxanthine phosphoribosyltransferase 1 (*Hprt1*) was used as the housekeeping gene.

The primers were designed using Primer3^{22,23} and synthesized by Eurofins (Eurofins Genomics, Ebersberg bei, München, Germany). To identify

the outliers of each group, Grubbs test for outliers (GraphPad Prism 8.0.2 for Windows GraphPad Prism Software, La Jolla, CA)²⁴ was applied on the cycle threshold (Ct) difference (ΔCt), calculated as $\Delta\text{Ct} = \text{Ct}_{\text{target}} - \text{Ct}_{\text{hprt1}}$ for each gene. Calculation of relative expression was derived from the $2^{-\Delta\Delta\text{Ct}}$ method using the relative expression software tool (REST version 2.07).²⁵

Chromatin Immunoprecipitation

Standard chromatin immunoprecipitation (ChIP) protocol was performed on atria of TG or WT mice.¹⁹ Eight to 10 animals were used from each of the 4 groups. The tissue was fixed with 1% formaldehyde, and chromatin was fragmented to 700 to 1000 bp by sonication and immunoprecipitated with a rabbit polyclonal anti-hemagglutinin tag (2.5 μg , ab9110 Abcam, Cambridge, UK) antibody. After purification and amplification of the whole genomic DNA, qRT-PCR was performed using primers designed around possible functional cAMP response element identified using JASPAR 2016²⁶ in the promoters of genes of interest. Glyceraldehyde-3-phosphate dehydrogenase was used as reference. The primers used to probe the specific promoter are described in Data S1.

The primers were designed using Primer3 software, as mentioned previously.

Measurement of Atrial Contraction

Left atria of all 4 experimental groups of mice were dissected in oxygenated ice-cold physiological solution and attached to a force transducer for recording isometric contractions electrically driven by field stimulation at 1 Hz using suprathreshold rectangular pulses of 5-millisecond duration, as described previously.²⁷ Before the experimental protocol, atria were prestretched with a force of 5 mN and were allowed to equilibrate at 37°C for at least 30 minutes in the bath solution and continuously oxygenated containing the following (in mmol/L): 120 NaCl, 5.4 KCl, 1.8 CaCl₂, 1 MgCl₂, 22.6 NaHCO₃, 0.42 NaH₂PO₄, 0.28 ascorbic acid, 0.05 Na₂EDTA, and 5.5 glucose adjusted to pH 7.4 with NaOH. To build the dose-response curves, the concentrations of carbachol or isoproterenol were increased every 5 minutes to the following concentrations (in mol/L) while the force of contraction was monitored continuously: 10⁻⁹, 10⁻⁸, 3 × 10⁻⁸, 10⁻⁷, 3 × 10⁻⁷, 10⁻⁶, 10⁻⁵, and 10⁻⁴ mol/L. Dose-response curves were built using the force of contraction measured for each concentration at steady state. Six of 12 WT_{6w} and 10 of 24 WT_{12w} mice atria did not show a positive staircase in response to isoproterenol application after carbachol; therefore, these results were excluded from the calculation of half-maximal effective concentration.

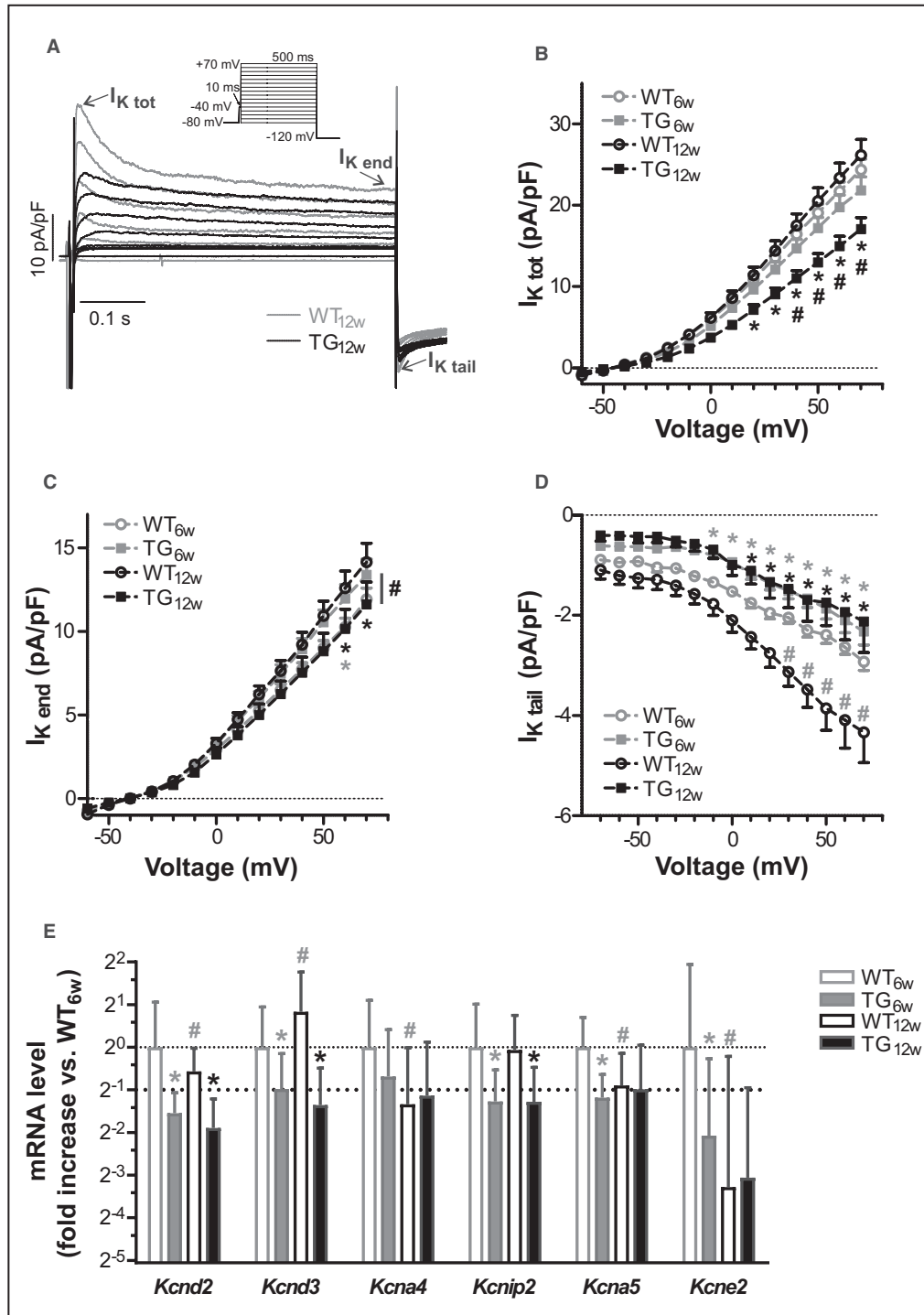
Statistical Analysis

Data are reported as mean ± SE. The number of cells is indicated by n, and the number of animals by N. Normal distribution was assessed using the Shapiro–Wilk test in GraphPad 8.0 (GraphPad Software, La Jolla, CA). According to the Gaussian distribution, Student *t* test, Mann–Whitney test, or Wilcoxon matched-pairs signed-rank test were used for 2-group comparisons, and 1-way analysis of variance test with Newman–Keuls post hoc test or Kruskal–Wallis test with the Dunn post hoc test were used for multiple-group comparisons. Current–voltage relation and dose-response curves were compared using 2-way repeated-measures analysis of variance with the Bonferroni post hoc test. Relative gene expression ratios were expressed as mean values ± SE for qRT-PCR and ChIP experiments as reported by the relative expression software tool REST (version 2.07).²⁵ Data were considered significantly different at *P* < 0.05.

RESULTS

Animal Model Characterization

CREM-IbΔC-X TG mouse, a well-established model for AF,¹¹ is characterized by extensive remodeling at the electrical and structural levels. In the present study, in vivo ECGs were performed on isoflurane-anesthetized young (6 weeks, TG_{6w}) and older (12 weeks, TG_{12w}) TG and age-matched WT to confirm the absence or presence of AF with age. TG mice revealed the AF-typical absence of the P-wave accompanied by a regular or irregular rhythm in 25% of TG_{6w} mice and more than 95% of TG_{12w} mice. For a small number of mice, 3.5% (2 of 57) TG_{12w} displayed no detectable P-wave, a flat isoelectric line, and a regular rhythm, and this pattern was not considered AF positive in this study. Applying these criteria, among 36 analyzed ECGs from the TG_{6w} group, we could detect 5 AF-positive mice (13.9%). Although in the WT_{6w} mice we could not detect any abnormal ECG recordings, in the WT_{12w} mice we identified only in 1 of 34 mice (2.9%) an ECG trace with no P-wave and regular heart rhythm. Representative ECG recordings from the TG mice and the analysis of the heart rate variability is presented in Figure S1A through S1F. The parameters of heart rate variability indicated no significant change of the mean heart rate in the TG_{12w} mice with AF versus age-matched controls and a significant increase of standard deviation of RR intervals in the mice with AF (Figure S1G–S1I). Overall, although confirmatory, these data indicate a low incidence of P-wave abnormalities in control mice and a good correlation between AF presence and the absence of P-wave and heart rate variability.



The structural remodeling of TG atria consists of enlarged atrial chambers and an elongated AM.^{11,15} The cells used in this study for the electrophysiological characterization were isolated from TG_{6w} mice with regular rhythms and from AF-positive TG_{12w} mice. We measured larger values of membrane capacitance (expressed in picofarads [pF]), as a cell-size index, in TG versus WT both at 6 weeks, when the ECGs of TG were AF negative (WT_{6w}: 69±6 pF,

n=59 versus TG_{6w}: 99±8 pF, n=42; $P<0.05$) and at 12 weeks, when the ECGs of TG were AF positive (WT_{12w}: 57±3 pF, n=61 versus TG_{12w}: 112±7 pF, n=36; $P<0.001$). The resting membrane potential (RMP) measured in isolated AM was -57.8±1 mV (WT_{6w}, n/N=40/15), -54.9±1.1 mV (TG_{6w}, n/N=44/18; $P=0.057$ versus WT_{6w}), -56.9±0.8 mV (WT_{12w}, n/N=64/25), and -52.1±1.2 mV (TG_{12w}, n/N=74/28; $P=0.007$ versus WT_{12w}). These results are in line with previously

Figure 1. Total K⁺ currents of transgenic atrial myocytes.

Experimental animals involved wild-type mice (WT) and transgenic mice (TG) expressing the repressor isoform of cyclic adenosine monophosphate response element modulator, CREM-IbΔC-X, and were distributed according to age in 6-week-old (WT_{6w} and TG_{6w}) and 12-week-old (WT_{12w} and TG_{12w}) groups. **A**, Representative K⁺ currents recorded from atrial myocytes of WT_{12w} and TG_{12w} using the voltage protocol illustrated in the inset. For clarity, current density (measured in picoamperes/picofarads [pA/pF]) traces from -40 mV with +20 mV increments are displayed. **B** through **D**, Mean±SE of current–voltage plots of peak total outward K⁺ current (I_{Ktot}) (**B**), total outward K⁺ current at the end of the pulse (I_{Kend}) (**C**), and tail K⁺ current (I_{Ktail}) (**D**). For WT_{6w}, n/N are 54/17 (**B** and **C**) and 45/17 (**D**), for TG_{6w}, n/N are 32/18 (**B** and **C**) and 31/18 (**D**), for WT_{12w}, n/N are 31/16 (**B** and **C**) and 29/15 (**D**), and for TG_{12w}, n/N are 22/14 (**B** and **C**) and 17/11 (**D**). **E**, Data show mean±SE of relative mRNA levels of the displayed genes normalized to WT_{6w} vs *Hprt1* (hypoxanthine phosphoribosyltransferase 1) as the housekeeping gene. Y-axes scale is Log2. N=8 per group except for K⁺ voltage-gated channel subfamily A member 5 (*Kcna5*) WT_{6w}, where N=7. **P*<0.05 TG_{6w} vs WT_{6w} (gray), TG_{12w} vs WT_{12w} (black), #*P*<0.05 WT_{12w} vs WT_{6w} (gray), TG_{12w} vs TG_{6w} (black) from 2-way repeated-measures analysis of variance with Bonferroni post hoc test (**B** through **D**) or as reported by REST 2.07 software (**E**).

reported increased membrane surface attributed to lengthening of the cells already present in TG_{6w} before AF onset and with the findings of depolarized myocytes in TG_{12w} investigated using sharp electrode intracellular recordings.¹⁵

Decreased K⁺ Currents in TG AM

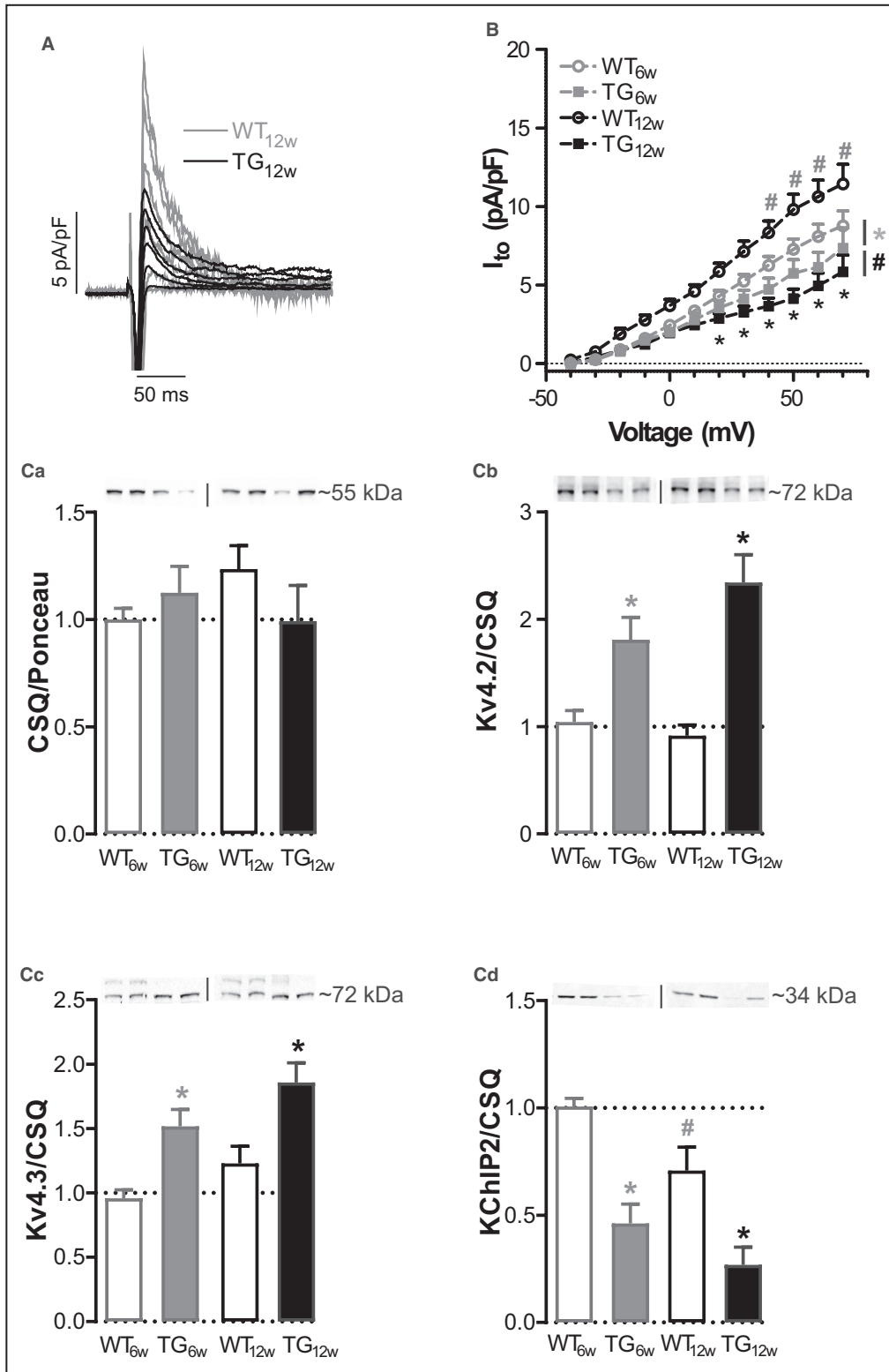
The electrical phenotype of the TG AM consisted of prolonged APD, as previously reported^{15,16} and as also shown in Figure S2. Based on previously reported reduced mRNA levels of some voltage-dependent K⁺ channel subunits in TG atria, we hypothesized that the slower repolarization may result from the reduced K⁺ efflux. Figure 1A compares representative K⁺ currents recorded from WT_{12w} and TG_{12w} AM using the voltage protocol displayed in the inset. The outward current was quantified as the (1) peak total outward K⁺ current at the beginning of the depolarizing pulse, composed of the transient outward current (I_{to}) and fast-activating slow-inactivating K⁺ current (I_{Kslow}), (2) the total outward K⁺ current at the end of the pulse (I_{Kend}) composed of fast-activating slow-inactivating K⁺ current (I_{Kslow}) and slow-activating slow-inactivating delayed rectifier K⁺ current (I_{Ks}), and (3) the peak inward current at -120 mV (tail K⁺ current [I_{Ktail}]) representing the tail currents of I_{Kend} plus the rapidly activating and inactivating delayed rectifier I_{Kr} .²⁸ The averaged current–voltage relations (I–V plots; Figure 1B–1D) show decreased peak total outward K⁺ current and I_{Kend} in TG_{12w} versus both WT_{12w} and TG_{6w}, whereas I_{Ktail} was reduced in TG versus WT at both ages. The significant increase of I_{Ktail} from WT_{6w} to WT_{12w} as a result of maturation was not present in TG. These results show different degrees of alterations of the major repolarizing K⁺ currents and suggest a greater contribution of I_{to} and I_{Kr} to the changes of peak total outward K⁺ current and I_{Ktail} , respectively.

To understand the molecular basis of K⁺ current alterations, we evaluated the mRNA levels of several genes encoding for α and β subunits of the classical K⁺ channels with roles in AP repolarization. Previously, using microarray experiments we detected decreased mRNA levels for K⁺ voltage-gated channel subfamily H

member 2 (*Kcnh2*, encoding the channel conducting I_{Kr}) and K⁺ voltage-gated channel subfamily Q member 1 (*Kcnq1*, encoding the channel conducting I_{Ks}) in TG versus WT mice at both ages.¹⁶ Here, we tested the expression of new genes encoding for other α and β subunits of the K⁺ channels and also confirmed by qRT-PCR the genes of interest, previously reported as downregulated.¹⁶ Figure 1E shows that mRNAs encoding for K⁺ voltage-gated channel subfamily D member 2 and 3 (*Kcnd2* and *Kcnd3*, encoding the fast component of I_{to} , I_{tof}), K⁺ voltage-gated channel interacting protein 2 (*Kcnip2* encoding for, β -auxiliary subunit KChIP2), but not of K⁺ voltage-gated channel subfamily A member 4 (*Kcna4*, encoding the slow component of I_{to} , I_{tos}), were reduced in TG versus WT mice, irrespective of age. In addition, before and not after AF onset, mRNA levels of K⁺ voltage-gated channel subfamily A member 5 (*Kcna5*, the main component of I_{Kslow}) and K⁺ voltage-gated channel subfamily E regulatory subunit 2 (*Kcne2*, encoding the β -auxiliary subunits KCNE2) were reduced by 2-fold in TG_{6w} versus WT_{6w} mice. These differences were not present after AF onset likely related to the downregulation of these genes in WT_{12w} versus WT_{6w} mice. We measured further WT-specific developmental changes such as reduced *Kcnd2* and *Kcna4* mRNA levels and a moderate upregulation of *Kcnd3* mRNA. In comparison, most of the genes downregulated in TG before AF remained at similar levels after AF. Overall, our data showed altered expression of different α and β subunits of K⁺ channels, suggesting that several molecular mechanisms such as the expression level and/or the biophysical properties of K⁺ channels contribute to the decrease of K⁺ currents.

Reduced I_{to} in TG AM

To confirm I_{to} reduction in TG, we applied the classical voltage protocol containing a prepulse to -40 mV to inactivate the channel.²⁹ Figure 2A illustrates representative I_{to} traces in WT_{12w} and TG_{12w} myocytes. The I–V plots show moderately reduced I_{to} in TG_{6w} versus WT_{6w}, developmentally increased I_{to} in WT_{12w} versus WT_{6w}, and reduced I_{to} in TG_{12w} versus both WT_{12w} and TG_{6w} (Figure 2B).



Next, we quantified the protein levels of the α subunits Kv4.2 and Kv4.3 and the β subunit KCHIP2, subunits underlying I_{to} using calsequestrin as a reference gene for myocyte content (Figure 2Ca–2Cd and Figure S3). On average, the reference protein calsequestrin showed similar levels among groups, Kv4.2 and Kv4.3 levels were increased, whereas

in line with the *Kcnp2* mRNA levels, KCHIP2 levels were reduced in TG versus age-matched WT, without differences within genotypes. Increased α -subunit expression in combination with lower KCHIP2 levels strongly suggest that impaired trafficking to the membrane surface³⁰ may contribute to the reduced I_{to} in TG atria.

Figure 2. Transient outward K⁺ channel expression in transgenic atrial myocytes.

Experimental animals involved wild-type mice (WT) and transgenic mice (TG) expressing the repressor isoform of cyclic adenosine monophosphate response element modulator, CREM-IbΔC-X, and were distributed according to age in 6-week-old (WT_{6w} and TG_{6w}) and 12-week-old (WT_{12w} and TG_{12w}) groups. **A**, Representative transient outward K⁺ current (I_{to}) traces recorded as -40 mV sensitive currents from atrial cardiomyocytes of WT_{12w} and TG_{12w}. For clarity, current density (expressed in picoamperes/picofarads [pA/pF]) traces from -40 mV with +20 mV increments are displayed. **B**, Mean±SE of current-voltage plots of the peak current density (I_{to}). For WT_{6w}, n/N are 41/15, for TG_{6w}, n/N are 22/14, for WT_{12w}, n/N are 35/19, and for TG_{12w}, n/N are 20/16. **Ca** through **d**, Representative immunoblots and quantification of protein expression of calsequestrin (CSQ; **Ca**) normalized to Ponceau and of K⁺ voltage-gated channel subfamily D member 2 (Kv4.2, **Cb**) and 3 (Kv4.3, **Cc**), and K⁺ channel interacting protein 2 (KChIP2) (**Cd**) normalized to CSQ. Data show mean±SE of N=7 mice per group, except for Kv4.3, where N=6 as the result of an undetectable band in TG_{12w}. *P<0.05 TG_{6w} vs WT_{6w} (gray), TG_{12w} vs WT_{12w} (black), #P<0.05 WT_{12w} vs WT_{6w} (gray), TG_{12w} vs TG_{6w} (black) from 2-way repeated-measures analysis of variance with Bonferroni post hoc test (**B**) and parametric or nonparametric 1-way analysis of variance with the corresponding post hoc test (**C**).

Reduced Inward Rectifier K⁺ Current in TG AM

Using hyperpolarizing voltage pulses, we found a significant reduction of the total inward K⁺ current in TG_{12w} versus both WT_{12w} and TG_{6w} (Figure S4). Under these experimental conditions, the inward K⁺ current results from K⁺ flowing through the inward rectifier K⁺ channel (K_{IR}, conducting the current I_{K1}), and the G-protein coupled inwardly rectifying K⁺ channel (GIRK) active at baseline. To assess only I_{K1}, a ramp protocol³¹ was applied in the presence and absence of 10 μmol/L BaCl₂ (Figure 3Aa). The mean I-V plots corresponding to the Ba²⁺-sensitive current (I_{K1}) (Figure 3Ab) confirmed I_{K1} reduction in TG_{12w}. As shown in Figure 3Ab, atrial I_{K1} displays a persistent outward component attributed to Kir2.1 heteromerization with the Kir2.3 α subunit, which is essential for the role of I_{K1} to AP repolarization and RMP stability.³² In Figure 3Ab, I_{K1} outward currents were not different between WT_{6w} and TG_{6w}, but significantly reduced in TG_{12w} versus WT_{12w}. The mRNA (Figure 3B) and protein (Figure 3Ca-3Cc) levels of K⁺ voltage-gated channel subfamily J member 2 (*Kcnj2*) and K⁺ inwardly rectifying channel α subunit 2.1 (Kir2.1), respectively, were decreased in TG versus WT at both ages, whereas K⁺ voltage-gated channel subfamily J member 4 (*Kcnj4*) and the corresponding K⁺ inwardly rectifying channel α subunit 2.3 (Kir2.3) were significantly reduced only after AF onset in TG_{12w} versus WT_{12w}, in line with the absence of the outward component in TG_{12w}. Next, we estimated the role of I_{K1} to RMP and AP repolarization in TG myocytes in the presence of BaCl₂. Representative AP traces recorded in the absence and presence of BaCl₂ are shown in Figure 3Da. The quantification of 10 μmol/L BaCl₂ effects on AP parameters (Figure S5) showed that BaCl₂ prolonged significantly the AP versus baseline (normal Tyrode [NT]) in WT_{6w}, TG_{6w}, and WT_{12w}, except for TG_{12w}. Figure 3Db presents the percentage of Ba²⁺-induced APD prolongation at 50% and 90% repolarization and shows that the magnitude of APD change of TG_{6w} myocytes was in the same range as for WT_{6w}, whereas TG_{12w} myocytes responded with a smaller change from the baseline. Following I_{K1} block by BaCl₂, RMP was depolarized

to -36.7±1.8 mV (WT_{6w}, n=7; P<0.05 BaCl₂ versus NT), -37.4±2.8 mV (TG_{6w}, n=5; P<0.05 BaCl₂ versus NT), -32±6.3 mV (WT_{12w}, n=5; P<0.05 BaCl₂ versus NT), and to -42.1±6.9 mV (TG_{12w}, n=3; P=0.095 BaCl₂ versus NT). Overall, these results show that I_{K1} contributed to both early and late repolarization of murine atrial AP and that in TG_{12w} the BaCl₂-induced AP changes were in line with reduced I_{K1} levels.

Reduced GIRK Channel Expression and Acetylcholine-Activated K⁺ Current in TG AM

The cardiac GIRK channel mediates the vagal effect on the heart electrical activity.³³ To determine whether the downregulation of K⁺ voltage-gated channel subfamily J member (*Kcnj3*) and 5 (*Kcnj5*) genes¹⁶ alters GIRK function, we recorded the K⁺ current activated by 10 μmol/L acetylcholine (I_{KACH}) as shown in Figure 4Aa. The mean I-V plots of I_{KACH} were reduced both for the inward and outward currents in TG versus WT irrespective of age (Figure 4Ab). The mRNA (Figure 4B) and protein (Figure 4Ca through 4Cc) levels of the corresponding α subunits 1 (*Kcnj3*/GIRK1) and 4 (*Kcnj5*/GIRK4) were reduced in the atria of TG versus age-matched WT, without differences between TG_{12w} and TG_{6w}.

Next, we measured AP in the presence of 10 μmol/L acetylcholine to test whether the reduction of I_{KACH} affects the autonomic regulation of atrial electrical activity. Representative AP traces recorded in the absence and presence of acetylcholine are shown in Figure 4Da. AP measurements showed that 10 μmol/L acetylcholine shortened significantly atrial AP both at 50% and at 90% repolarization in all groups except for TG_{6w} (Figures 4Db and S5). Following I_{KACH} activation by acetylcholine, RMP was hyperpolarized to -66±0.6 mV (WT_{6w}, n=8; P<0.05 acetylcholine versus NT), -62.8±2.1 mV (TG_{6w}, n=4; not significant acetylcholine versus NT), -65.9±2.2 mV (WT_{12w}, n=7; P<0.05 acetylcholine versus NT) and to -65±4.3 mV (TG_{12w}, n=3; P=0.083 acetylcholine versus NT). The response of TG_{12w} to acetylcholine was similar to WT_{12w}, whereas in comparison to TG_{6w}, TG_{12w} AM showed the tendency to elicit a larger response to acetylcholine (P=0.082,

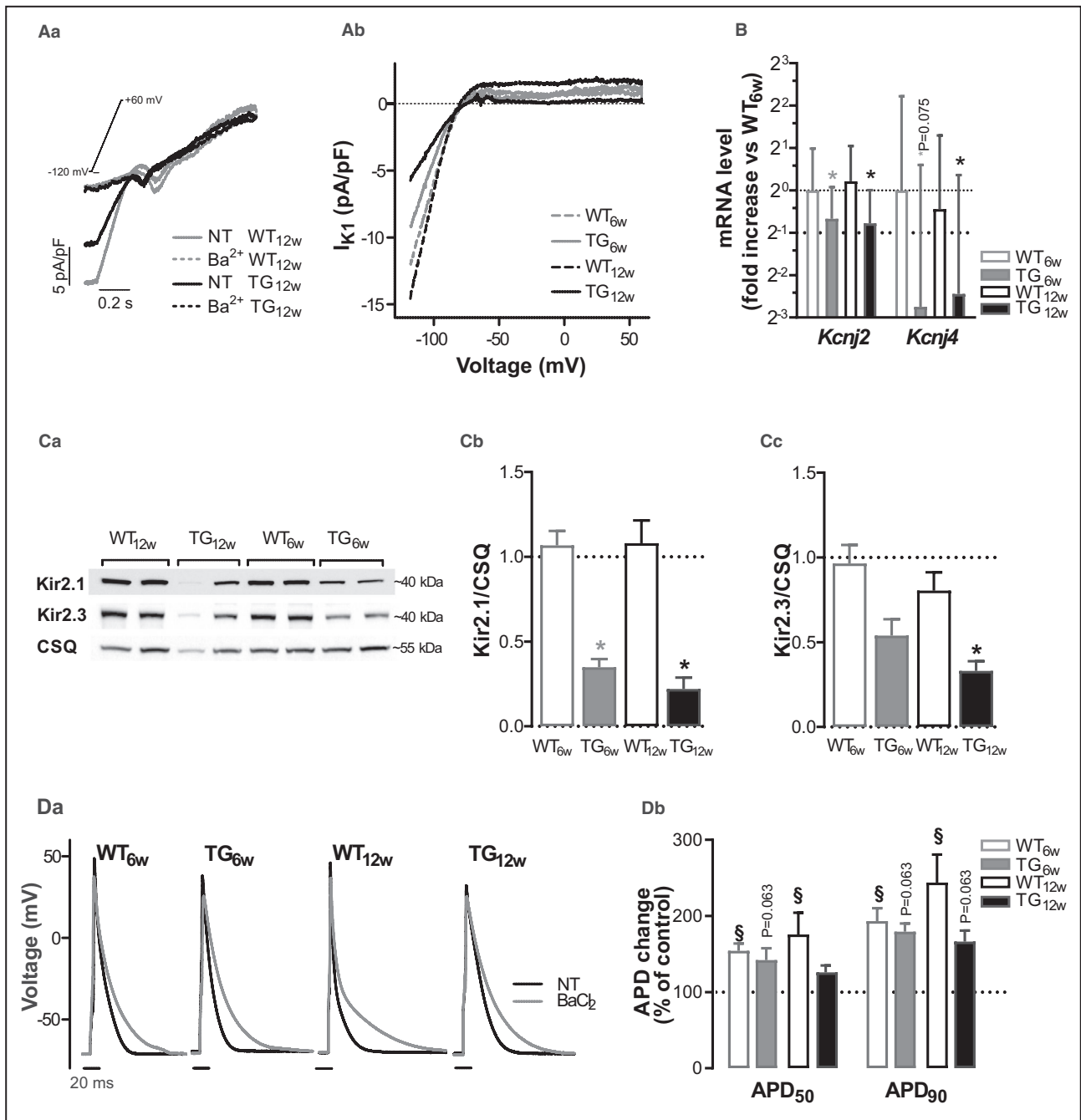


Figure 3. Inward rectifier K⁺ current I_{K1} expression and function in transgenic atrial myocytes.

Experimental animals involved wild-type mice (WT) and transgenic mice (TG) expressing the repressor isoform of cyclic adenosine monophosphate response element modulator, CREM-IbΔC-X, and were distributed according to age in 6-week-old (WT_{6w} and TG_{6w}) and 12-week-old (WT_{12w} and TG_{12w}) groups. **A**, Representative traces of inward rectifiers K⁺ channel (I_{K1}) recorded in WT_{12w} and TG_{12w} myocytes before and after application of 10 μmol/L BaCl₂ using a ramp protocol (inset, scale bar 0.2 seconds). The traces show current density (expressed in picoamperes/picofarads [pA/pF]) over time. (**Aa**). Current-voltage plots of I_{K1} averaged from traces of all cells. For WT_{6w}, n/N are 8/5, for TG_{6w} n/N are 10/6, for WT_{12w} n/N are 13/7, and for TG_{12w} n/N are 9/6 (**Ab**). **B**, Data show mean±SE of relative mRNA levels of atrial K⁺ voltage-gated channel subfamily J member 2 (*Kcnj2*) and 4 (*Kcnj4*) normalized to WT_{6w} vs *Hprt1* (hypoxanthine phosphoribosyltransferase 1) as the housekeeping gene; N=8 per group. Y-axis scale is Log2. **Ca** through **c**, Representative immunoblots (**Ca**) and quantification of K⁺ inwardly rectifying channel subunits Kir2.1 (**Cb**) and Kir2.3 (**Cc**) protein levels normalized to calsequestrin (CSQ). Data show mean±SE of 7 mice per group. **Da** through **b**, Representative action potentials recorded before (normal Tyrode [NT]) as control) and after application of 10 μmol/L BaCl₂ in 1 atrial myocyte of each group (**Da**). Quantification of the percentages of action potential duration (APD) change in BaCl₂ vs NT at 50% (APD₅₀) and 90% (APD₉₀) repolarization. Data show mean±SE of n/N for WT_{6w} (7/5), TG_{6w} (5/5), WT_{12w} (11/6), and TG_{12w} (5/4) (**Db**). *P<0.05 TG_{6w} vs WT_{6w} (gray) and TG_{12w} vs WT_{12w} (black) (**A** through **C**) from 2-way repeated-measures analysis of variance with Bonferroni post hoc test (**Ab**), REST 2.07 software (**B**), and parametric or nonparametric 1-way analysis of variance with the corresponding post hoc test (**C**); §P<0.05 BaCl₂ vs NT using Wilcoxon matched-pairs signed-rank test (**Db**).

Bonferroni post hoc test, 2-way analysis of variance). These data suggest that despite similar I_{KACH} , GIRK contributes to AP shortening more in TG_{12w} than TG_{6w}.

CREM-Dependent Gene Transcription

Next, we used ChIP to test if the α subunits with reduced mRNA levels were directly regulated by the transcription repressor CREM. The results presented in Figure 5 correspond to 6-week-old (Figure 5A) and 12-week-old (Figure 5B) mice. The data showed that *Kcnd2*, *Kcnd3*, *Kcnj3*, and *Kcnh2* genes were enriched in TG versus WT irrespective of age, whereas *Kcna5* DNA binding ratio showed a strong trend only in TG_{6w}. For *Kcnj2*, *Kcnj4*, and *Kcnj5*, we could not detect an increased DNA binding ratio despite reduced mRNA levels at both ages. As validated CREM target genes,^{34,35} *FBJ Murine Osteosarcoma Viral Oncogene Homolog (c-fos)* and small inducible adenosine monophosphate early repressor (*smIcer*) were significantly enriched in TG versus age-matched WT. These data show that *Kcnd2*, *Kcnd3*, *Kcnj3*, and *Kcnh2* were directly regulated by CREM-IbΔC-X that may explain the reduction of mRNA levels before AF onset.

Left Atrial Contraction Response to Autonomic Nervous System

I_{KACH} data suggested an altered parasympathetic regulation of TG hearts. To better understand the autonomic regulation of the TG heart, we measured the changes of the atrial force of contraction (FOC) to increasing concentrations of the muscarinic M₂-receptor (M₂R) agonist carbachol or of the β -adrenoceptor (β AR) agonist isoproterenol. Because the right atria of TG showed extremely reduced FOC that would not allow us to evaluate the intrinsic electrical automatism of the sino-atrial node, only the left atria were used for further experiments. Figure 6 shows reduced FOC in TG atria already before AF onset that decreased further by 45% in TG_{12w} versus TG_{6w}, in line with the massive structural disorganization of the myofilaments and also with the reduced synchronization of individual cell contractions as a result of increased conduction heterogeneity.^{15,16} Next, FOC was measured in response to increasing concentrations of carbachol (Figure 7A) or of isoproterenol (Figure 7B) to assess the individual sensitivities to parasympathetic and sympathetic stimulation in TG_{12w} left atria. Dose-response curves for carbachol showed reduced efficacy in TG_{12w} versus WT_{12w}, without shifting the dose-response curves (half maximal inhibitory concentration [nM]: WT_{12w}, 72±19, N=8; TG_{12w}, 102±66, N=8; not significant; Figure 7Ac). In contrast, dose-response curves to isoproterenol showed increased efficacy in TG_{12w} versus WT_{12w}, without shifting the dose-response

curves (half-maximal effective concentration [nM]: WT_{12w}, 295±33, N=10; TG_{12w}, 243±19, N=10; not significant; Figure 7Bc). These results show that despite reduced contraction, TG atria were able to respond to both carbachol and isoproterenol stimulation with the same sensitivity as WT_{12w}.

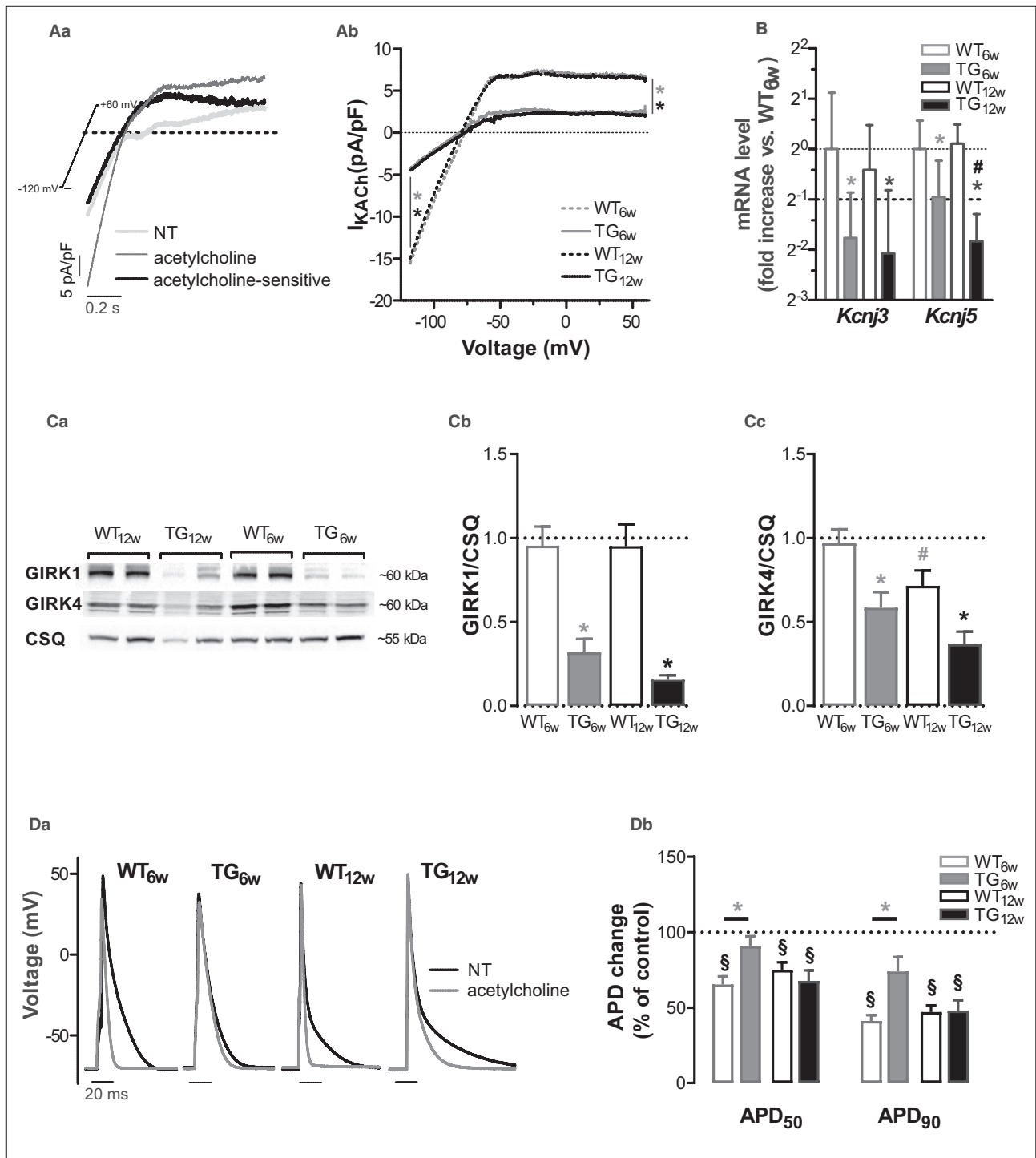
Simultaneous sympathetic-vagal activation associates with AF onset better than alterations in vagal or sympathetic drive alone.³⁶ Therefore, we evaluated FOC in response to combined M₂R and β AR stimulation. M₂R activation was adjusted to 50% using 300 nmol/L carbachol before application of increasing concentrations of isoproterenol (Figure 8A). Under these conditions, isoproterenol increased FOC to levels that were no further different between genotypes. In relation to initial FOC, isoproterenol increased atrial contraction up to 177.7% and 220% above the baseline in TG_{6w} and TG_{12w}, respectively, significantly more versus age-matched WT, where on average, isoproterenol did not exceed the inhibitory effect of 300 nmol/L carbachol (Figure 8B). The normalized responses to isoproterenol were shifted to the left for TG_{6w} and TG_{12w} versus age-matched WT (half-maximal effective concentration [μ mol/L]: WT_{6w}, 6.7±0.9, N=6; TG_{6w}, 0.64±0.06, N=10 [$P<0.05$]; and WT_{12w}, 5±0.7, N=14; TG_{12w}, 0.77±0.38, N=12 [$P<0.05$]; Figure 8C). These data show that in a combined vagal-sympathetic stimulation, TG atria displayed increased sensitivity and contraction to β AR stimulation irrespective of AF onset.

DISCUSSION

This is the first study describing the electrical remodeling of K⁺ currents in CREM-IbΔC-X TG AM. In TG_{6w} before AF onset, we found (1) reduced I_{to} and I_{KACH} , (2) increased sympathetic sensitivity attributed to reduced parasympathetic antagonism, and (3) absent vagal-induced APD shortening. These alterations explain the APD prolongation at 50%¹⁶ and the increased AF inducibility of TG_{6w}.¹⁵ In TG_{12w}, simultaneous with persistent AF, we found additionally (1) reduced I_{K1} , (2) further reduction of I_{to} , and (3) the presence of vagal-induced APD shortening. These changes explain the depolarized RMP,¹⁵ the additional APD lengthening,¹⁶ and the increased electrical heterogeneity,¹⁵ all mechanisms involved in AF stabilization.¹ Furthermore, the results that *Kcnd2*, *Kcnd3*, *Kcnh2*, and *Kcnj3* were direct target genes of CREM-IbΔC-X demonstrate for the first time that CREM activity directly contributes to proarrhythmic electrical remodeling in atria.

CREM-Induced Electrical Alterations and Potential Link to AF

TG mice display extensive structural and metabolic remodeling of atria.¹⁶ Our present data showed that



electrical remodeling was accompanied by low mRNA levels for *Kcnd2*, *Kcnd3*, *Kcnp2*, *Kcna5*, *Kcnj2*, *Kcnj4*, *Kcnj3*, and *Kcnj5* already in TG_{6w} versus WT_{6w}, which did not change significantly with further phenotype progression in TG_{12w} versus TG_{6w}. ChIP experiments confirmed that *Kcnd2*, *Kcnd3*, *Kcnh2*, and *Kcnj3* were target genes of CREM-IbΔC-X, suggesting that these genes may be directly linked to cAMP response element-mediated transcription. It remains to be

determined whether *Kcnj2*, *Kcnj4*, or *Kcnj5* downregulation may involve an indirect CREM-dependent regulation via mechanisms requiring CREM dimerization with other transcription factors.³⁷

I_{to} Reduction in TG Atria

The reduction of I_{to} is a hallmark of hypertrophy and was linked to APD prolongation in atrial pathologies

Figure 4. Acetylcholine-activated K⁺ current (I_{KACH}) expression and function in transgenic atrial myocytes.

Experimental animals involved wild-type mice (WT) and transgenic mice (TG) expressing the repressor isoform of cyclic adenosine monophosphate response element modulator, CREM-IbΔC-X, and were distributed according to age in 6-week-old (WT_{6w} and TG_{6w}) and 12-week-old (WT_{12w} and TG_{12w}) groups. **A**, Representative traces recorded before and after application of 10 μmol/L acetylcholine using the ramp protocol (inset, scale bar 0.2 seconds) in 1 isolated WT_{12w} atrial cardiomyocyte. The acetylcholine-sensitive current derived by subtraction is I_{KACH}. The traces show current density (expressed in picoamperes/picofarads [pA/pF]) over time. **(Aa)**, Current-voltage plots of I_{KACH} averaged from traces of all cells. n/N for WT_{6w} are 12/6, for TG_{6w} are 13/7, for WT_{12w} are 12/6, and for TG_{12w} are 10/6 **(Ab)**. **B**, Relative mRNA levels of K⁺ voltage-gated channel subfamily J members 3 (*Kcnj3*) and 5 (*Kcnj5*) measured in atrial tissue, with *Hprt1* (hypoxanthine phosphoribosyltransferase 1) as the housekeeping gene. Data were normalized to WT_{6w}. Y-axis scale is Log2. Data show mean±SE of 8 per group. **Ca** through **c**, Representative immunoblots **(Ca)** and quantification of G protein-coupled inwardly rectifying K⁺ channel α subunits 1 (GIRK1, **Cb**) and 4 (GIRK4, **Cc**) protein levels normalized to calsequestrin (CSQ). Data show mean±SE of N=7 mice per group. **Da** through **b**, Representative action potentials recorded before (normal Tyrode [NT] as control) and after application of 10 μmol/L acetylcholine in 1 atrial myocyte of each group **(Da)** and quantification of the percentage of action potential duration (APD) change in acetylcholine vs NT at 50% (APD₅₀) and 90% (APD₉₀) repolarization. Data show mean±SE of n/N for WT_{6w} (9/5), TG_{6w} (5/5), WT_{12w} (11/6), and TG_{12w} (6/4) **(Db)**. *P<0.05 TG_{6w} vs WT_{6w} (gray) and TG_{12w} vs WT_{12w} (black) and #P<0.05 WT_{12w} vs WT_{6w} (gray) and TG_{12w} vs TG_{6w} (black) **(A through C)** from 2-way repeated-measures analysis of variance with Bonferroni post hoc test **(Ab)**, REST 2.07 software **(B)**, and parametric or nonparametric 1-way analysis of variance with the corresponding post hoc test **(C)**. §P<0.05 acetylcholine vs NT. *P<0.05 as shown using Wilcoxon matched-pairs signed-rank test **(Db)**.

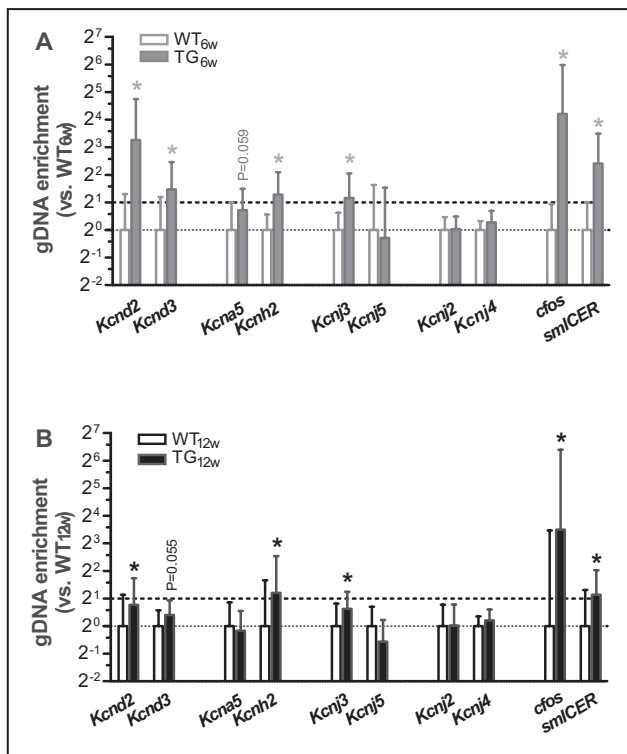


Figure 5. Cyclic adenosine monophosphate response element modulator (CREM)-dependent gene expression.

A and **B**, Chromatin immunoprecipitation results for selected genes: K⁺ voltage-gated channel subfamily D member 2 (*Kcnd2*) and 3 (*Kcnd3*), K⁺ voltage-gated channel subfamily A member 5 (*Kcna5*), K⁺ voltage-gated channel subfamily H member 2 (*Kcnh2*), K⁺ voltage-gated channel subfamily J member 3 (*Kcnj3*), 5 (*Kcnj5*), 2 (*Kcnj2*) and 4 (*Kcnj4*), FBJ Murine Osteosarcoma Viral Oncogene Homolog (*c-fos*) and small inducible adenosine monophosphate early repressor (*smIcER*). Bar graphs show mean±SE of genomic DNA (gDNA) enrichment at 6 weeks **(A)** and 12 weeks **(B)** of age in transgenic mice (TG) expressing the repressor isoform of cyclic adenosine monophosphate response element modulator, CREM-IbΔC-X, vs age-matched wild-type mice (WT). N=7–8 for WT_{6w}, N=8 for TG_{6w}, N=7–8 for WT_{12w}, and N=9–10 for TG_{12w}. *P<0.05 TG_{6w} vs WT_{6w} (gray) and TG_{12w} vs WT_{12w} (black) calculated by REST 2.07 software.

including atrial dilatation³⁸ and AF.³⁹ In line with AM increased size (hypertrophy) of TG_{6w}, we found moderate reduction of I_{to} before AF onset. I_{to} decreased even more in TG_{12w}, opposite to I_{to} increase in WT atria. Developmental I_{to} increase was reported in normal mouse ventricle,⁴⁰ and our results suggest a mechanism based on the isoform switch from *Kcnd2* to *Kcnd3* in WT atria, which was impaired in TG_{12w}, in line with the identification of *Kcnd3* as CREM-target gene. Although consistent with decreased mRNA

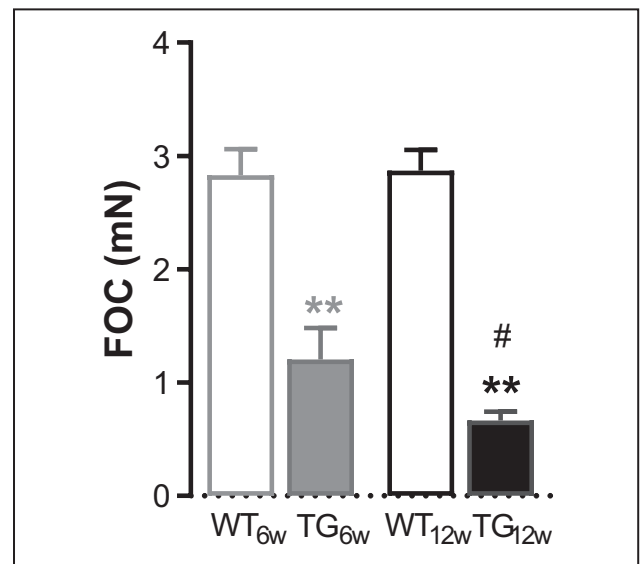


Figure 6. Left atrial contraction of transgenic mice (TG) expressing the repressor isoform of cyclic adenosine monophosphate response element modulator, CREM-IbΔC-X.

Force of contraction (FOC) measured in the left atria. Experimental animals involved wild-type (WT) and TG animals distributed according to age in 6-week-old (WT_{6w} and TG_{6w}) and 12-week-old (WT_{12w} and TG_{12w}) groups. Data show mean±SE of mice from WT_{6w} (N=12), TG_{6w} (N=10), WT_{12w} (N=49), and TG_{12w} (N=47). **P<0.01 TG_{6w} vs WT_{6w} (gray) and TG_{12w} vs WT_{12w} (black) and #P<0.05 TG_{12w} vs TG_{6w} (black) from the Kruskal–Wallis test with the Dunn post hoc test.

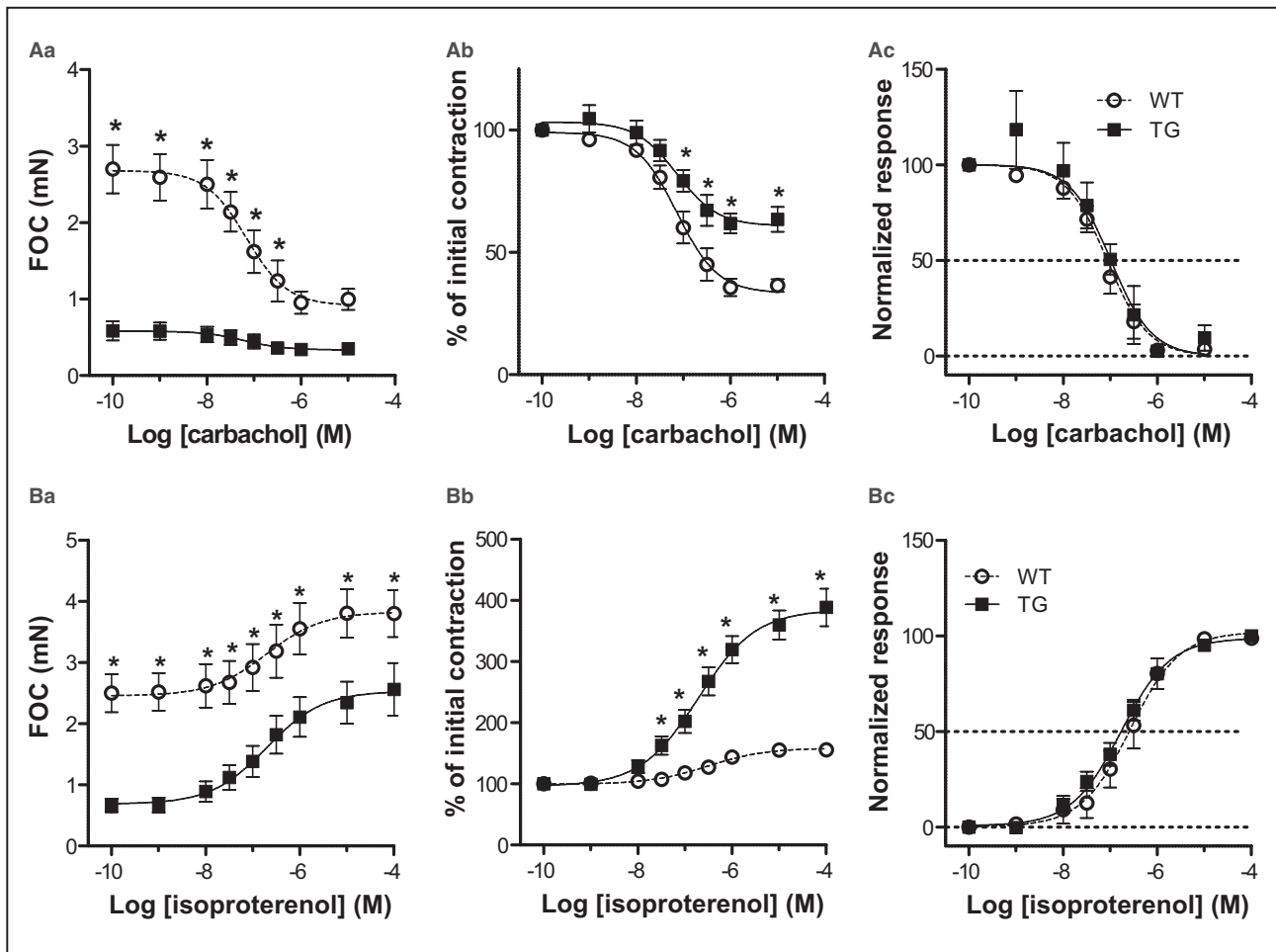


Figure 7. Dose-response curve of left atrial contraction in response to autonomic stimulation.

Experimental animals involved wild-type mice (WT) and transgenic mice (TG) expressing the repressor isoform of cyclic adenosine monophosphate response element modulator, CREM-IbΔC-X, and were distributed according to age in 6-week-old (WT_{6w} and TG_{6w}) and 12-week-old (WT_{12w} and TG_{12w}) groups. **A**, Force of contraction (FOC) of the left atria was measured in WT_{12w} and TG_{12w} mice under increasing concentrations of carbachol. Data show mean±SE of raw FOC (**Aa**), normalized to baseline value (**Ab**), and normalized to minimum (in carbachol 10⁻⁵ mol/L) and maximum (before carbachol) FOC (**Ac**). For WT_{12w} N is 8 and for TG_{12w} N is 8. **B**, FOC of left atria was measured in WT_{12w} and TG_{12w} mice under increasing concentrations of isoproterenol. Data show mean±SE of raw FOC (**Ba**), normalized to initial FOC (**Bb**), and normalized to minimum (before isoproterenol) and maximum (in isoproterenol 10⁻⁴ mol/L) FOC (**Bc**). For WT_{12w} N is 10 and for TG_{12w} N is 10. *P<0.05 TG_{12w} vs WT_{12w} from 2-way repeated-measures analysis of variance with Bonferroni post hoc test.

levels of *Kcnd2* and *Kcnd3*, I_{to} reduction in TG was not supported by the increased protein levels of Kv4.2/3, but more by mechanisms involving KChIP2. A cAMP response element has been reported in the promoter region of KChIP2, and together with the observations that KChIP2 reduction parallels the reduction of CREB activity following rapid pacing of canine hearts, and the finding that I_{to} is absent in canine myocytes injected with a CREB antisense virus, a link is established between the activity of CREB and I_{to} levels via KChIP2.^{41,42} It is possible that *Kcnip2* is a target gene of both CREB (inductor) and CREM (repressor) and, therefore, may explain why CREM overexpression decreased mRNA levels of *Kcnip2*, similar to a reduction of CREB activity. In contrast to

these findings, KChIP2 was unaltered in ventricular myocytes of heart-specific CREB knockout mice,²¹ a different mouse model where the absence of CREB may have a different impact on the regulation of *Kcnip2* gene transcription or may be compensated by other members of the CREB/CREM/ATF1 family. Here, we showed that KChIP2 expression was reduced both at mRNA and protein levels in TG atria, suggesting that different mechanisms regulating gene transcription may exist between atrial and ventricular tissues as well as depending on the model employed. Because the role of KChIP2 protein in Kv4.2/3 trafficking to the plasma membrane³⁰ is well accepted, these results suggest that KChIP2 down-regulation is one mechanism for impaired trafficking

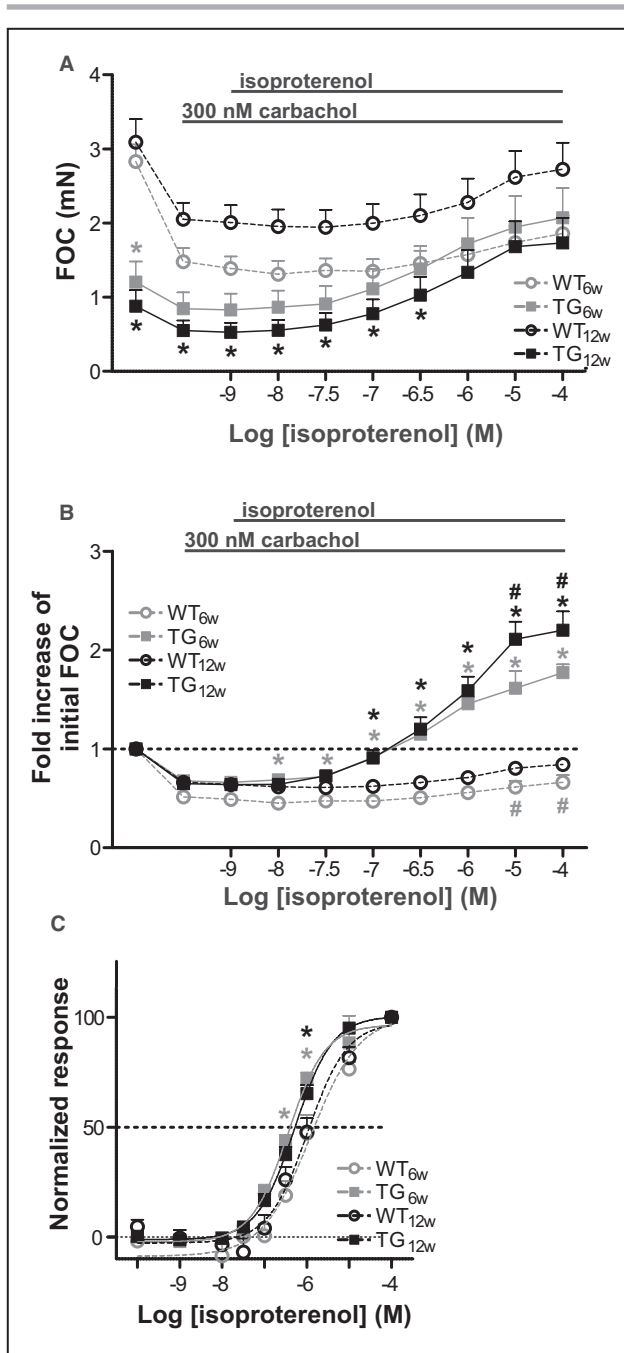


Figure 8. The effect of functional antagonism of vagal-sympathetic stimulation on left atrial contraction of transgenic mice (TG) expressing the repressor isoform of cyclic adenosine monophosphate response element modulator, CREM-IbΔC-X. Experimental animals involved wild-type (WT) and TG animals distributed according to age in 6-week-old (WT_{6w} and TG_{6w}) and 12-week-old (WT_{12w} and TG_{12w}) groups. **A** through **C**, Force of contraction (FOC) of left atria measured before and under continuous presence of 300 nmol/L carbachol during the application of increasing isoproterenol concentrations. Data show mean±SE of raw FOC (**A**), FOC normalized to initial FOC (**B**), and FOC normalized to minimum (300 nmol/L carbachol) and maximum (10⁻⁴ mol/L isoproterenol) FOC (**C**). Mice from WT_{6w} (N=12), TG_{6w} (N=10), WT_{12w} (N=24), and TG_{12w} (N=13) (**A** and **B**) and from WT_{6w} (N=6), TG_{6w} (N=10), WT_{12w} (N=14), and TG_{12w} (N=12) were included (**C**). *P<0.05 TG_{6w} vs WT_{6w} (gray) and TG_{12w} vs WT_{12w} (black) and #P<0.05 WT_{12w} vs WT_{6w} and TG_{12w} vs TG_{6w} (black) from 2-way repeated-measures analysis of variance with Bonferroni post hoc test.

at 50%¹⁶ and increased AF inducibility to stimuli such as high pacing¹⁵ or to sympathetic stimulation as shown for hypertrophied ventricular myocytes, but it does not explain the spontaneous AF or the further APD prolongation at 90% lengthening after AF onset. Thus, alterations of other currents such as I_{Ks}, I_{Kr}, I_{K1}, and I_{KACH} may contribute to late repolarization phase of atrial AP.⁴⁵

Inward Rectifier Expression in TG Atria and Their Contribution to AF

I_{K1} and I_{KACH} have important roles for heart physiology such as maintaining a stable RMP and mediating the parasympathetic modulation of the electrical activity, respectively.^{32,33} Both currents contribute to AP repolarization as a result of their outward component. In pathology, the increase of I_{K1} and/or I_{KACH} associated better with AF because they induce atrial AP shortening that will abbreviate the effective refractory period and therefore facilitate electrical re-entrance and AF perpetuation.⁴⁶ In our mice with spontaneous AF, our main finding was that both these inward rectifiers, I_{K1} and I_{KACH}, were reduced at the current, protein, and mRNA levels. These data suggest a fine control of the activity of the inward rectifier K⁺ channels because both downregulation and upregulation may support AF. The reduction of I_{K1} is proarrhythmic because it induces an decrease of membrane conductance at rest. As a consequence, small depolarizing stimuli that otherwise may not reach the electrical threshold for AP generation will create larger depolarizations and trigger APs that may lead to destabilization of the membrane potential leading to cardiac arrhythmia.⁴⁷ As for I_{KACH}, GIRK activation increases the resting conductance therefore hyperpolarizes the membrane and reduces the response to threshold stimuli, thus mediating the parasympathetic negative chronotropic and bathmotropic effect of acetylcholine at

of K⁺ channels to plasma membrane, additional to the previously reported disorganized cytoskeleton and decreased levels of ankyrin B and G in TG atria.¹⁶ However, the direct link between I_{to} and the proarrhythmic atrial phenotype is not fully understood because the targeted deletion of *Kcnd2* showed no changes in ECG regarding P-wave or propensity to arrhythmia,⁴³ whereas combined decrease of I_{to} and I_{KACH} were reported in the left atrial posterior wall, a region associated with increased ectopic activity.⁴⁴ Therefore, we consider that the decrease of I_{to} in the atria of TG mice explains some changes that appeared before AF onset such as APD prolongation

the sino-atrial and atrial levels, respectively. A smaller $I_{K_{ACH}}$ would not be able to hyperpolarize the RMP to the same extent, thus enabling arrhythmia. Our results relate to cases of patients with long QT syndrome type 7 (Andersen-Tawil syndrome) and long QT syndrome 13 where mutations of *Kcnj2* and *Kcnj5* led to decreased I_{K1} and $I_{K_{ACH}}$, respectively. These long QT syndromes were associated with atrial torsade de point in a canine model of Andersen-Tawil syndrome⁴⁸ and high incidence of atrial arrhythmia,⁴⁹ respectively. Moreover, decreased mRNA levels of *Kcnj2*, *Kcnj3*, and *Kcnj5* were reported in an arrhythmia-susceptible atrial region of normal mice⁴⁴ and in atria of murine models of AF and heart failure.^{8,50} Except for the left atrial posterior wall where I_{K1} was not changed and $I_{K_{ACH}}$ was reduced, neither the levels of these currents nor the levels of *Kcnj4/Kir2.3* were assessed in these animal models. Here, we showed that *Kcnj4/Kir2.3* downregulations occurred after AF onset in CREM TG mice, and this change explains the reduction of outward component of I_{K1} that significantly contributed to APD prolongation at 90% in AF-positive mice and likely to the depolarized RMP.¹⁵ Although the role of I_{K1} to AP repolarization was in line with the current measurements, the acetylcholine effect on APD was different in TG_{12w} versus TG_{6w}, despite a similar current density of $I_{K_{ACH}}$ before and after AF. This effect will be discussed later.

Based on computer simulations, I_{K1} reduction induced a compensatory larger contribution of I_{Kr} to repolarization,⁵¹ leading to the hypothesis that patients with Andersen-Tawil syndrome may display susceptibility to arrhythmias when both I_{K1} and I_{Kr} are reduced,⁴⁷ a situation that may be present in TG atria. As in the absence of I_{K1} the contribution of I_{Kr} to repolarization increases,⁵¹ when I_{Kr} is reduced, I_{Ks} acts as repolarizing reserve for I_{Kr} .⁴⁷ Although we did not focus on pharmacological separation of I_{Kr} and I_{Ks} , our results suggested I_{Kr} reduction in TG mice as a result of reduced $I_{K_{tail}}$ at similar levels of $I_{K_{end}}$, lower *Kcnh2* mRNA levels,¹⁶ and enrichment of genomic *Kcnh2* DNA in ChIP experiments. Moreover, the lower mRNA levels of *Kcnq1*¹⁶ would suggest a decreased I_{Ks} likely part of the decreased $I_{K_{end}}$ of TG_{12w}. Different mechanisms may contribute to arrhythmia as a result of APD prolongation. The increased incidence of early afterdepolarization after sympathetic stimulation has been described for I_{to} -induced APD lengthening, whereas for I_{K1} reduction, the corresponding AP prolongation may result in delayed afterdepolarizations triggered by Na⁺/Ca²⁺ exchanger.⁵² All of these results suggest that in TG_{12w}, the combined reduction of I_{K1} , $I_{K_{ACH}}$, I_{Kr} , and I_{Ks} additionally to I_{to} decline depleted significantly the repolarization reserve currents and contributed to further APD prolongation at 90% and increased susceptibility to arrhythmia.⁵¹

Autonomic Regulation of TG Atria

It has been postulated that the changes in the autonomic nervous system activity increase susceptibility to AF and reversely that AF itself may shift the autonomous system activation,³⁶ establishing a positive feedback loop. Here, we showed that under combined vagal-sympathetic stimulation TG atria manifested increased sensitivity to catecholamines, suggesting a reduced antagonism of the parasympathetic over sympathetic system. We propose that at an unopposed sympathetic activation may lead to heart rhythm dysregulations at the sino-atrial node such as tachycardia and tachyarrhythmias and to early or delayed afterdepolarizations and increased ectopic activities in AM on a background of RMP instability attributed to I_{K1} reduction, prolonged APD, and the APD shortening as a result of vagal stimulation. In line with increased sensitivity to sympathetic innervation are the previous in vivo studies on TG mice showing increased ventricular contractility under basal conditions in hemodynamic measurements.¹¹ The use of a preparation of right atria to evaluate the autonomic regulation of the sino-atrial node of TG was impaired by the extremely reduced FOC and the large size of the atria in the mice with AF. At atrial level, the regain of $I_{K_{ACH}}$ ability to shorten APD after AF onset would contribute to a shorter effective refractory period and increased heterogeneity of the electrical activity, mechanisms described as drivers for AF perpetuation.^{36,44} The differences between the acetylcholine-induced APD shortening before and after AF onset may result from altered coupling between M₂R and GIRK or different basal activities of GIRK.⁵³ This could imply that $I_{K_{ACH}}$ contributes more to basal APD of TG_{6w} and not of TG_{12w}, therefore opening new questions for further in-depth studies addressing the characterization of the cholinergic system in TG mice. Our results suggest that the presence of acetylcholine-induced APD shortening at ages where AF is already present may be an additional mechanism to the proarrhythmic alterations discussed previously. Thus, the presence of the ability of vagal stimulation to reduce the effective refractory period may create another substrate for electrical rotors' stabilization and AF perpetuation in TG_{12w}. The lack of vagal-induced APD shortening together with normal I_{K1} levels may partly explain the absence of spontaneous AF in TG_{6w}. Overall, our data implied that although the reduced vagal effect is present before AF onset, atria require an RMP destabilizer such as I_{K1} reduction to trigger and maintain AF.

CONCLUSIONS

Our study identified a complex electrical remodeling that contributes to AP prolongation and AF maintenance in CREM-IbΔC-X atria consisting of decreased I_{to} , I_{K1} , and $I_{K_{ACH}}$ and increased sensitivity to sympathetic

stimulation. Many K⁺ currents linked to familial forms of long QT syndrome^{49,54} were identified as target genes of CREM-IbΔC-X, suggesting that their overlapped down-regulation created an electrical substrate for AF in CREM TG mouse. Here, we propose a direct link between CREM activation and atrial failure-associated electrical remodeling and suggest new molecular targets for future therapeutic strategies for AF treatment.

ARTICLE INFORMATION

Received February 10, 2020; accepted September 29, 2020.

Affiliations

From the Institute of Pharmacology and Toxicology, University of Münster, Münster, Germany.

Acknowledgments

We acknowledge Stefanie Triebel, Maria Schulik, Franzis Volkery, Melanie Voß, Danuta Mitko, and Nina Goda for excellent technical assistance and Dr. Jan S. Schulte for the Origin 8.1 Macro for action potential duration (APD) analysis. We acknowledge support from the Open Access Publication Fund of the University of Muenster. Open access funding enabled and organized by Projekt DEAL.

Sources of Funding

This study was funded by the European Union (Framework Program 7 [FP7] European Commission FP7-HEALTH-2010 European Network for Translational Research in Atrial Fibrillation to Dr Müller) and the Deutsche Forschungsgemeinschaft (Mu1376/11–3 to Dr Müller).

Disclosures

None.

Supplementary Material

Data S1

Figures S1–S5

REFERENCES

- Schotten U, Verheule S, Kirchhof P, Goette A. Pathophysiological mechanisms of atrial fibrillation: a translational appraisal. *Physiol Rev*. 2011;91:265–325.
- Gaspo R, Bosch RF, Talajic M, Nattel S. Functional mechanisms underlying tachycardia-induced sustained atrial fibrillation in a chronic dog model. *Circulation*. 1997;96:4027–4035.
- Wijffels MC, Kirchhof CJ, Dorland R, Allesie MA. Atrial fibrillation begets atrial fibrillation. A study in awake chronically instrumented goats. *Circulation*. 1995;92:1954–1968.
- Rivard AL, Suwan PT, Imaninaini K, Gallegos RP, Bianco RW. Development of a sheep model of atrial fibrillation for preclinical prosthetic valve testing. *J Heart Valve Dis*. 2007;16:314–323.
- Bauer A, McDonald AD, Donahue JK. Pathophysiological findings in a model of persistent atrial fibrillation and severe congestive heart failure. *Cardiovasc Res*. 2004;61:764–770.
- Wan E, Abrams J, Weinberg RL, Katchman AN, Bayne J, Zakharov SI, Yang L, Morrow JP, Garan H, Marx SO. Aberrant sodium influx causes cardiomyopathy and atrial fibrillation in mice. *J Clin Invest*. 2016;126:112–122.
- Pan Z, Ai T, Chang PC, Liu Y, Liu J, Maruyama M, Homsy M, Fishbein MC, Rubart M, Lin SF, et al. Atrial fibrillation and electrophysiology in transgenic mice with cardiac-restricted overexpression of FKBP12. *Am J Physiol Heart Circ Physiol*. 2018;316:H371–H379.
- Rommel C, Rosner S, Lothar A, Barg M, Schwaderer M, Gilsbach R, Bomicke T, Schnick T, Mayer S, Doll S, et al. The transcription factor *etv1* induces atrial remodeling and arrhythmia. *Circ Res*. 2018;123:550–563.
- Ma JF, Yang F, Mahida SN, Zhao L, Chen X, Zhang ML, Sun Z, Yao Y, Zhang YX, Zheng GY, et al. Tbx5 mutations contribute to early-onset atrial fibrillation in Chinese and Caucasians. *Cardiovasc Res*. 2016;109:442–450.
- Perez-Hernandez M, Matamoros M, Barana A, Amoros I, Gomez R, Nunez M, Sacristan S, Pinto A, Fernandez-Aviles F, Tamargo J, et al. Pitx2c increases in atrial myocytes from chronic atrial fibrillation patients enhancing I_{Ks} and decreasing I_{CaL}. *Cardiovasc Res*. 2016;109:431–441.
- Muller FU, Lewin G, Baba HA, Boknik P, Fabritz L, Kirchhefer U, Kirchhof P, Loser K, Matus M, Neumann J, et al. Heart-directed expression of a human cardiac isoform of camp-response element modulator in transgenic mice. *J Biol Chem*. 2005;280:6906–6914.
- Muller FU, Boknik P, Knapp J, Neumann J, Vahlensieck U, Oetjen E, Scheld HH, Schmitz W. Identification and expression of a novel isoform of camp response element modulator in the human heart. *FASEB J*. 1998;12:1191–1199.
- Li N, Chiang DY, Wang S, Wang Q, Sun L, Voigt N, Respress JL, Ather S, Skapura DG, Jordan VK, et al. Ryanodine receptor-mediated calcium leak drives progressive development of an atrial fibrillation substrate in a transgenic mouse model. *Circulation*. 2014;129:1276–1285.
- Deshmukh A, Barnard J, Sun H, Newton D, Castel L, Pettersson G, Johnston D, Roselli E, Gillinov AM, McCurry K, et al. Left atrial transcriptional changes associated with atrial fibrillation susceptibility and persistence. *Circ Arrhythm Electrophysiol*. 2015;8:32–41.
- Kirchhof P, Marijon E, Fabritz L, Li N, Wang W, Wang T, Schulte K, Hanstein J, Schulte JS, Vogel M, et al. Overexpression of camp-response element modulator causes abnormal growth and development of the atrial myocardium resulting in a substrate for sustained atrial fibrillation in mice. *Int J Cardiol*. 2013;166:366–374.
- Seidl MD, Stein J, Hamer S, Pluteanu F, Scholz B, Wardelmann E, Hüge A, Witten A, Stoll M, Hammer E, et al. Characterization of the genetic program linked to the development of atrial fibrillation in *crem-ibΔC-X* mice. *Circ Arrhythm Electrophysiol*. 2017;10:e005075.
- Jansen HJ, Mackasey M, Moghtadaei M, Liu Y, Kaur J, Egom EE, Tuomi JM, Rafferty SA, Kirkby AW, Rose RA. NPR-C (natriuretic peptide receptor-C) modulates the progression of angiotensin II-mediated atrial fibrillation and atrial remodeling in mice. *Circ Arrhythm Electrophysiol*. 2019;12:e006863. <https://doi.org/10.1161/CIRCEP.118.006863>
- Kirchhof P, Eckardt L, Franz MR, Monnig G, Loh P, Wedekind H, Schulze-Bahr E, Breithardt G, Haverkamp W. Prolonged atrial action potential durations and polymorphic atrial tachyarrhythmias in patients with long QT syndrome. *J Cardiovasc Electrophysiol*. 2003;14:1027–1033.
- Scholz B, Schulte JS, Hamer S, Himmler K, Pluteanu F, Seidl MD, Stein J, Wardelmann E, Hammer E, Volker U, et al. HDAC (histone deacetylase) inhibitor valproic acid attenuates atrial remodeling and delays the onset of atrial fibrillation in mice. *Circ Arrhythm Electrophysiol*. 2019;12:e007071. <https://doi.org/10.1161/CIRCEP.118.007071>
- Stumpel FT, Stein J, Himmler K, Scholz B, Seidl MD, Skryabin BV, Muller FU. Homozygous *crem-ibΔC-X* overexpressing mice are a reliable and effective disease model for atrial fibrillation. *Front Pharmacol*. 2018;9:706.
- Schulte JS, Seidl MD, Nunes F, Freese C, Schneider M, Schmitz W, Muller FU. Creb critically regulates action potential shape and duration in the adult mouse ventricle. *Am J Physiol Heart Circ Physiol*. 2012;302:H1998–H2007.
- Rozen S, Skaletsky H. Primer3 on the www for general users and for biologist programmers. *Methods Mol Biol*. 2000;132:365–386.
- Untergasser A, Cutcutache I, Koressaar T, Ye J, Faircloth BC, Remm M, Rozen SG. Primer3—new capabilities and interfaces. *Nucleic Acids Res*. 2012;40:e115.
- Grubbs FE. Procedures for detecting outlying observations in samples. *Technometrics*. 1969;11:1–21.
- Vandesompele J, De Preter K, Pattyn F, Poppe B, Van Roy N, De Paeppe A, Speleman F. Accurate normalization of real-time quantitative RT-PCR data by geometric averaging of multiple internal control genes. *Genome Biol*. 2002;3:RESEARCH0034.
- Mathelier A, Fornes O, Arenillas DJ, Chen CY, Denay G, Lee J, Shi W, Shyr C, Tan G, Worsley-Hunt R, et al. JASPAR 2016: A major expansion and update of the open-access database of transcription factor binding profiles. *Nucleic Acids Res*. 2016;44:D110–D115.
- Heinick A, Husser X, Himmler K, Kirchhefer U, Nunes F, Schulte JS, Seidl MD, Rolfe C, Dedman JR, Kaetzel MA, et al. Annexin A4 is a novel direct regulator of adenylyl cyclase type 5. *FASEB J*. 2015;29:3773–3787.
- Nakamura H, Ding WG, Sanada M, Maeda K, Kawai H, Maegawa H, Matsuura H. Presence and functional role of the rapidly activating

- delayed rectifier K(+) current in left and right atria of adult mice. *Eur J Pharmacol.* 2010;649:14–22.
29. Brouillette J, Clark RB, Giles WR, Fiset C. Functional properties of k+ currents in adult mouse ventricular myocytes. *J Physiol.* 2004;559:777–798.
 30. Foeger NC, Marionneau C, Nerbonne JM. Co-assembly of kv4 alpha subunits with k+ channel-interacting protein 2 stabilizes protein expression and promotes surface retention of channel complexes. *J Biol Chem.* 2010;285:33413–33422.
 31. Rinne A, Littwitz C, Kienitz MC, Gmerek A, Bosche LI, Pott L, Bender K. Gene silencing in adult rat cardiac myocytes in vitro by adenovirus-mediated rna interference. *J Muscle Res Cell Motil.* 2006;27:413–421.
 32. Dharmoon AS, Pandit SV, Sarmast F, Parisian KR, Guha P, Li Y, Bagwe S, Taffet SM, Anumonwo JM. Unique kir2.X properties determine regional and species differences in the cardiac inward rectifier k+ current. *Circ Res.* 2004;94:1332–1339.
 33. Cha TJ, Ehrlich JR, Chartier D, Qi XY, Xiao L, Nattel S. Kir3-based inward rectifier potassium current: potential role in atrial tachycardia remodeling effects on atrial repolarization and arrhythmias. *Circulation.* 2006;113:1730–1737.
 34. Seidl MD, Nunes F, Fels B, Hildebrandt I, Schmitz W, Schulze-Osthoff K, Muller FU. A novel intronic promoter of the crem gene induces small icer (smicer) isoforms. *FASEB J.* 2014;28:143–152.
 35. Ginty DD, Bonni A, Greenberg ME. Nerve growth factor activates a Ras-dependent protein kinase that stimulates c-fos transcription via phosphorylation of CREB. *Cell.* 1994;77:713–725.
 36. Linz D, Elliott AD, Hohl M, Malik V, Schotten U, Dobrev D, Nattel S, Bohm M, Floras J, Lau DH, et al. Role of autonomic nervous system in atrial fibrillation. *Int J Cardiol.* 2018;287:181–188.
 37. Iourgenko V, Zhang W, Mickanin C, Daly I, Jiang C, Hexham JM, Orth AP, Miraglia L, Meltzer J, Garza D, et al. Identification of a family of camp response element-binding protein coactivators by genome-scale functional analysis in mammalian cells. *Proc Natl Acad Sci USA.* 2003;100:12147–12152.
 38. Le Grand BL, Hatem S, Deroubaix E, Couetil JP, Coraboeuf E. Depressed transient outward and calcium currents in dilated human atria. *Cardiovasc Res.* 1994;28:548–556.
 39. Van Wagoner DR, Pond AL, McCarthy PM, Trimmer JS, Nerbonne JM. Outward K+ current densities and kv1.5 expression are reduced in chronic human atrial fibrillation. *Circ Res.* 1997;80:772–781.
 40. Wang L, Duff HJ. Developmental changes in transient outward current in mouse ventricle. *Circ Res.* 1997;81:120–127.
 41. del Balzo U, Rosen MR. T wave changes persisting after ventricular pacing in canine heart are altered by 4-aminopyridine but not by lidocaine. Implications with respect to phenomenon of cardiac 'memory'. *Circulation.* 1992;85:1464–1472.
 42. Patberg KW, Obreztschikova MN, Giardina SF, Symes AJ, Plotnikov AN, Qu J, Chandra P, McKinnon D, Liou SR, Rybin AV, et al. The camp response element binding protein modulates expression of the transient outward current: implications for cardiac memory. *Cardiovasc Res.* 2005;68:259–267.
 43. Guo W, Jung WE, Marionneau C, Aimond F, Xu H, Yamada KA, Schwarz TL, Demolombe S, Nerbonne JM. Targeted deletion of kv4.2 eliminates i(to, f) and results in electrical and molecular remodeling, with no evidence of ventricular hypertrophy or myocardial dysfunction. *Circ Res.* 2005;97:1342–1350.
 44. Holmes AP, Yu TY, Tull S, Syeda F, Kuhlmann SM, O'Brien SM, Patel P, Brain KL, Pavlovic D, Brown NA, et al. A regional reduction in Ito and IKAch in the murine posterior left atrial myocardium is associated with action potential prolongation and increased ectopic activity. *PLoS One.* 2016;11:e0154077.
 45. Nerbonne JM, Kass RS. Molecular physiology of cardiac repolarization. *Physiol Rev.* 2005;85:1205–1253.
 46. Nattel S. Atrial electrophysiology and mechanisms of atrial fibrillation. *J Cardiovasc Pharmacol Ther.* 2003;8:S5–S11.
 47. Zipes DP, Jalife J. *Cardiac electrophysiology: from cell to bedside.* Philadelphia, PA: Elsevier/Saunders; 2014.
 48. Satoh T, Zipes DP. Cesium-induced atrial tachycardia degenerating into atrial fibrillation in dogs: atrial torsades de pointes? *J Cardiovasc Electrophysiol.* 1998;9:970–975.
 49. Bohnen MS, Peng G, Robey SH, Terrenoire C, Iyer V, Sampson KJ, Kass RS. Molecular pathophysiology of congenital long QT syndrome. *Physiol Rev.* 2017;97:89–134.
 50. Wiedmann F, Schulte JS, Gomes B, Zafeiriou MP, Ratte A, Rathjens F, Fehrmann E, Scholz B, Voigt N, Muller FU, et al. Atrial fibrillation and heart failure-associated remodeling of two-pore-domain potassium (K2P) channels in murine disease models: focus on TASK-1. *Basic Res Cardiol.* 2018;113:27.
 51. Seemann G, Sachse FB, Weiss DL, Ptacek LJ, Tristani-Firouzi M. Modeling of IK1 mutations in human left ventricular myocytes and tissue. *Am J Physiol Heart Circ Physiol.* 2007;292:H549–H559.
 52. Tristani-Firouzi M, Jensen JL, Donaldson MR, Sansone V, Meola G, Hahn A, Bendahhou S, Kwiecinski H, Fidzianska A, Plaster N, et al. Functional and clinical characterization of KCNJ2 mutations associated with LQT7 (andersen syndrome). *J Clin Invest.* 2002;110:381–388.
 53. Peleg S, Varon D, Ivanina T, Dessauer CW, Dascal N. G(alpha)(i) controls the gating of the G protein-activated K(+) channel, GIRK. *Neuron.* 2002;33:87–99.
 54. Amin AS, Tan HL, Wilde AA. Cardiac ion channels in health and disease. *Heart Rhythm.* 2010;7:117–126.

SUPPLEMENTAL MATERIAL

Data S1.

SUPPLEMENTAL METHODS

The data that support the findings of this study are available from the corresponding author upon reasonable request.

Materials

Unless otherwise stated, all reagents have been purchased from Sigma-Aldrich (Sigma-Aldrich Chemie GmbH, Munich, Germany).

Experimental animals

Mice with cardiomyocyte-directed overexpression of hemagglutinin (HA)-tagged CREM-Ib Δ C-X (CREM TG) were described previously^{11, 12}. Wild-type (WT) littermates have been used as control. Mice were kept at a room temperature of 22°C, under a 12-h light/dark cycle and received normal diet (Altromin Spezialfutter GmbH, Lage, Germany) and water *ad libitum*. The mice were euthanized by CO₂ inhalation. Animals were handled and maintained according to the rules of local welfare authority and the Directive 2010/63/EU of the European Parliament. The animals were grouped in 4 categories according to age (5-7 and 11-13 weeks) and genotype (WT and TG) as follows: WT_{6w}, TG_{6w}, WT_{12w} and TG_{12w}.

In vivo ECG measurements

Electrocardiogram (ECG) measurements were performed in isoflurane anesthetized mice to confirm the absence (in WT_{6w}, TG_{6w} and WT_{12w} mice) and the presence of persistent atrial fibrillation (in TG_{12w}). Mice were anesthetized with isoflurane (1.2% v/v) and nitrous oxide (66% v/v) while being placed on a warmed pad in supine position. Needle electrodes were attached to obtain limb leads (Einthoven). Short ECGs were recorded for 1 minute after achieving deep anesthesia (in 5 minutes) using a PowerLab hardware and LabChart Pro software (ADInstruments, Bella Vista, Australia). A section of 20 seconds at steady state of

the ECG recordings were analyzed offline using Heart Rate Variability module (HRV) to measure the following parameters: mean heart rate (HR), standard deviation of NN intervals (SDNN), root mean square of the successive differences between neighboring RR intervals (RMSSD). After ECG measurements the hearts were used for cell isolation or biochemical assays.

Tissue isolation

The hearts were removed in ice cold calcium free Tyrode's solution. Both atria were quickly cut from the heart, frozen in liquid nitrogen and stored for further analysis using qRT-PCR, Western blot and Chromatin immunoprecipitation (ChIP) assays.

Isolation of atrial cardiomyocytes

Atrial cardiomyocytes were isolated from all 4 groups of mice, using the retrograde perfusion of the hearts to digest the connective tissue with collagenase Type II (230U/mg; Worthington, Lakewood, NJ, USA) as described before¹⁶. The TG mice exhibiting AF at the age of 5-7 weeks were randomly detected with low incidence. Due to the small number and the aim of our study they were not included or sufficient for further investigation. Prior to cell isolation, it was essential to perform ECG measurements on all mice to test for AF presence or absence for grouping the data after analysis, therefore, not all experimenters were blinded. Moreover, due to the strong atrial phenotype, the quality of cell isolation was poor (few or no cells) in TG mice, meaning that more TG than WT mice had to be sacrificed for this study.

Electrophysiology

Ca²⁺-tolerant atrial myocytes were used for the measurements of ionic currents using the patch-clamp technique in perforated-patch configuration achieved with amphotericin B (300 µg/mL; Sigma-Aldrich Chemie GmbH, Steinheim, Germany). All recordings have been performed at room temperature (22-24 °C). Borosilicate glass capillaries (Science Products GmbH, Hofheim, Germany) were pulled to a resistance of 3-5MΩ with a horizontal puller (P-

97, Sutter Instruments Inc., Novato, CA, USA). Data were sampled with an 18-bit A/D converter InstruTech ITC-18 and filtered at 10 kHz using an EPC-800 amplifier under the control of the PatchMaster software (HEKA Elektronik, Lambrecht, Germany). The average values for the seal resistances: $1.35 \pm 0.15 \text{ G}\Omega$ (WT_{6w}, n = 56), $0.93 \pm 0.18 \text{ G}\Omega$ (TG_{6w}, n = 37), $1.09 \pm 0.13 \text{ G}\Omega$ (WT_{12w}, n = 56) and $1.07 \pm 0.24 \text{ G}\Omega$ (TG_{12w}, n = 32) were not significantly different between groups. The series resistances reached on average $22.9 \pm 1.6 \text{ M}\Omega$ (WT_{6w}, n = 56), $22.4 \pm 1.9 \text{ M}\Omega$ (TG_{6w}, n = 37), $23.2 \pm 1 \text{ M}\Omega$ (WT_{12w}, n = 56) and $22.6 \pm 1.3 \text{ M}\Omega$ (TG_{12w}, n = 32) and were compensated between 52 % and 66 % in order to insure the stability of the recordings. An average level of compensation of 55 % was achieved in each group. To record action potentials and K⁺-currents, the cells were perfused with a bath solution containing (in mM): 136 NaCl, 5.4 KCl, 1 CaCl₂, 1 MgCl₂, 5 HEPES, 0.33 NaH₂PO₄ and 10 glucose, adjusted to pH 7.4 with NaOH and the pipettes were filled with a solution containing (in mM): 5 NaCl, 120 KCl, 2.5 MgATP, 1 EGTA and 5 HEPES adjusted to pH 7.2 with KOH. The 10 μM solutions of BaCl₂ or acetyl choline (ACh) were freshly prepared from 100 mM BaCl₂ or 100 mM ACh, respectively, stock solutions in water.

To measure the total outward K⁺ currents, the cells were clamped at -80 mV followed by a 10 ms prepulse to -40 mV to inactivate the sodium channel and a series of 500 ms voltage steps from -80 to +70 mV in 10 mV increment. The depolarizing step was followed by a 300 ms pulse to -120 mV for assessing the inward tail currents flowing through the delayed rectifier currents, including HERG current (I_{Kr}). I_{Ktot} and I_{Kend} current amplitudes were measured as the peak current or the current at the end of the depolarizing pulse minus the mean current at -40 mV. The I_{Ktail} current amplitude was measured as the current at peak minus the current at the end of the 300 ms pulse to -120 mV. The transient outward channel (I_{to}) was inactivated using a 180 ms prepulse to -40 mV followed by a 5 s voltage steps from -

40 to +70 mV in 10 mV increment. The I_{to} currents were obtained after offline subtraction of the depolarizing steps of the two voltage protocols and the amplitudes were measured as peak current minus the current at the end for the subtracted trace. The inward rectifier I_{K1} current was measured as the current at the end of the 500 ms pulses between -120 and -10 mV from -40 mV holding voltage. To assess the $BaCl_2$ and ACh sensitive currents, a voltage ramp between -120 to +60 mV for 1 second, from the holding voltage of -40 mV was applied at 30 seconds interval. Action potentials (AP) were triggered at 1 Hz frequency with a suprathreshold current stimulus of 600 – 1000 pA amplitude and 3 - 6 ms duration. Three to five consecutive AP traces at steady state were averaged, and action potential amplitude, slope, and durations from the peak to 20, 50, 70 and 90 % repolarization using a macro for APD analysis designed by Dr. Jan S. Schulte (University of Münster, Germany)²¹ for Origin 8.1 (OriginLab Corporation, Northampton, MA, USA).

Western blot

Atria from six to eight mice have been used from each group. Both left and right atria were pooled from each mouse and homogenized in lysis buffer containing 100 mM NaCl, 20 mM Tris Base, 1% sodium deoxycholate, 0.1% SDS, 1% Triton X-100, pH adjusted to 8.0 and supplemented with phosphatase and protease inhibitor tablets (A32959, ThermoFischer Scientific, Darmstadt, Germany). Protein concentration of the homogenate was measured using the classical Bradford method (Thermo Fisher Scientific). The samples were equally distributed and 40 μ g of protein loaded per well of the 10% SDS-PAGE gel. Equal protein load was assessed after transfer using Ponceau stain. The following rabbit polyclonal primary antibodies were used: Kv4.2 (1:200, APC 023 Alomone Labs, Jerusalem, Israel), Kv4.3 (1:200, APC 017 Alomone Labs), KChIP2 (1:200, sc-25685, Santa Cruz Biotechnology Inc, CA, USA) Kir2.1 (1:200, APC 159, Alomone Labs), Kir2.3 (1:1000, APC 032, Alomone Labs), Kir3.1 (1:200, APC 005, Alomone Labs), Kir3.4 (1:200, APC 027, Alomone Labs) and

calsequestrin (CSQ, 1:2500, PA1-913, Thermo Fisher Scientific). As secondary antibodies we used HRP conjugated anti-rabbit IgG antibody (1:10000, A27036 Thermo Fisher Scientific) further developed with SERVALight Helios (42587.03, SERVA Electrophoresis GmbH, Heidelberg, Germany) or SERVALight Eos (42585.02, SERVA Electrophoresis GmbH). Band intensities were quantified using ImageJ 1.49v (National Institute of Health, Bethesda, MD, USA). Each band was normalized for load (to the Ponceau stain intensity of the full lane), for transfer (normalized to the reference considered the averaged signal of the WT_{6w} bands of the same membrane) and to CSQ for myocyte content. The normalized values of the samples belonging to the same group were averaged for statistical comparison.

Quantitative real time PCR (qRT-PCR)

Eight animals have been used from each group. Total RNA was purified using TRIzol (15596018, ThermoFisher Scientific) according to the manufacturer instructions, and 1 µg was reversely transcribed to cDNA that served as input for real-time PCR. The primers used to probe the ion channel subunits were as follows:

Kcnd2: for 5'-CTGCTCACGGAGACACAAAA-3';

rev 5'-CGGCTGTTGGATAGTGGAGT-3'

Kcnd3: for 5'-TGTACGAACCTCCACCATCA-3';

rev 5'-AGTGGCTGGACAGAGAAGGA-3'

Kcna4: for 5'-GAAGAAGGGGTCAAGGAATC-3';

rev 5'-TGGCAGGTGGAGAGAACAAT-3'

Kcnip2: for 5'-GACATGATGGGCAAGTACACC-3';

rev 5'-ACGCCGTCCTTGTCTGT-3'

Kcna5: for 5'-TCCGACGGCTGGACTCAATAA-3';

rev 5'-CAGATGGCCTTCTAGGCTGTG-3'

Kcnb1: for 5'-CCACCAGATTCTCCCACAGT-3';

rev 5'-GCTCTCCACGAAGAAACCAG-3'

Kcnq1: for 5'-GGCTACGGGGATAAGGTACC-3';

rev 5'-CACCTCCATGCAGTCTGGAT-3'

Kcnh2: for 5'-GTGGAGATCGCCTTCTACCG-3';

rev 5'-CCCTGTGGTTGGTGTCATGA-3'

Kcne1: for 5'-GCAGAGCCTCGACCATTTAG-3';

rev 5'-GTAGAGCGCCTCTAGCTTGC-3'

Kcne2: for 5'-CACATTAGCCAATTTGACCCAGA-3';

rev 5'-GAACATGCCGATCATCACCAT-3'

Kcnj2: for 5'-GGGAATTCTCACTTGCTTCG-3';

rev 5'-AGAGATGGATGCTTCCGAGA-3'

Kcnj3: for 5'-AGTAGAAAGGGGTCAGGCAC-3';

rev 5'-GGCCACCTCTTACCTTTCCA-3'

Kcnj4: for 5'-GACCCTCCTCGGACCTTA C-3';

rev 5'-GACGTTACACTGGCCGTTCT-3'

Kcnj5: for 5'-ATGTCTCGTGCTCAACTGGA-3';

rev 5'-AACTGGGTGTGTTGGTCTCA-3'

Hprt1: for 5'-ATGAGCGCAAGTTGAATCTG-3';

rev 5'-GGACGCAGCAACTGACATT-3'

Hypoxanthine phosphoribosyltransferase 1 (*Hprt1*) was used as housekeeping gene.

The primers were designed using Primer3^{22,23} and synthesized by Eurofins (Eurofins Genomics, Ebersberg bei München, Germany). The outliers in a group were calculated based on the dCt ($C_{t_{\text{target}}} - C_{t_{\text{hprt}}}$) for each gene using Grubbs' test for outliers (GraphPad Prism Version 8.0.2 for Windows, GraphPad Prism Software, La Jolla, California, USA).²⁴

Calculation of relative expression was derived from the $2^{-\Delta\Delta Ct}$ method using the relative expression software tool (REST© Version 2.07).²⁵

Chromatin immunoprecipitation (ChIP)

Standard ChIP protocol was performed on atria of TG or WT mouse¹⁹. Eight to ten animals have been used per group. The tissue was fixed with 1% formaldehyde, chromatin was fragmented to 700-1000 bp by sonication and immunoprecipitated with a rabbit polyclonal anti-HA antibody (tag, 2.5 µg, ab9110 Abcam, Cambridge, UK). After purification and amplification of the whole genomic DNA, real-time PCR was performed using primers designed around possible functional cyclic AMP response element (CRE) identified using JASPAR2016²⁶ in the promoters of genes of interest. Glyceraldehyde-3-phosphate dehydrogenase (GAPDH) was used as reference. The primers used to probe the specific promoter region were as follows:

Kcnd2: for 5'-TTTGGGAAGGTGACAAGGAG-3';

rev 5'-GGGGCTGAGTTGCATAGAGA-3'

Kcnd3: for 5'-TATTGGAGCGAATCCTGACC-3';

rev 5'-ATCCCACGGAAGACAAACTG-3'

Kcna5: for 5'-CGGTTTCCTCTTCAGCCGAG-3';

rev 5'-TGGTAACCAGCTGCCAGAAC-3'

Kcnh2: for 5'-ATGGTCGGTTTGGAGGTGAC-3';

rev 5'-ATTTTCTGGCTGTCCCCTGG-3'

Kcnj2: for 5'-CGTGTCAGAGGTCAACAGCT-3';

rev 5'-TTGCCATCTTCGCCATGACT-3'

Kcnj3: for 5'-GGGCGGACATGGAATAGGAG-3';

rev 5'-AATGCAGGTGTGTCAGGCTC-3'

Kcnj4: for 5'-ACGTTACACTGGCCGTTCTT-3';

rev 5'-GGTCTCCAAACCGTCCTCTG-3'

Kcnj5: for 5'-AAGCCAAAGAACAGCCAGGT-3';

rev 5'-ACATCCCCATTGCCACAGAC-3'

c-fos: for 5'-TGCCAAGACGGGGGTTGAAAG-3';

rev 5'-TGCAGTCGCGGTTGGAGTAGTAGG-3'

smICER: for 5'-TCTGCTCTTCAGCTAATTGAGTTCAAA-3';

rev 5'-GAAAGGAACTGACTAAATCACAACATGACT-3'

Gapdh: for 5'-TGCACCACCAACTGCTTA-3';

rev 5'-GGATGCAAGGATGATGTTTC-3'

The primers were designed using Primer3^{22,23} and synthesized by Eurofins (Eurofins Genomics, Germany). The outliers of each group were calculated based on the dCt ($C_{t_{target}} - C_{t_{hprt}}$) for each gene using Grubbs' test for outliers (GraphPad Prism Version 8.0.2 for Windows, GraphPad Prism Software, La Jolla, California, USA).²⁴ Calculation of relative expression was derived from the $2^{-\Delta\Delta C_t}$ method using the relative expression software tool (REST© Version 2.07)²⁵.

Measurement of atrial contraction

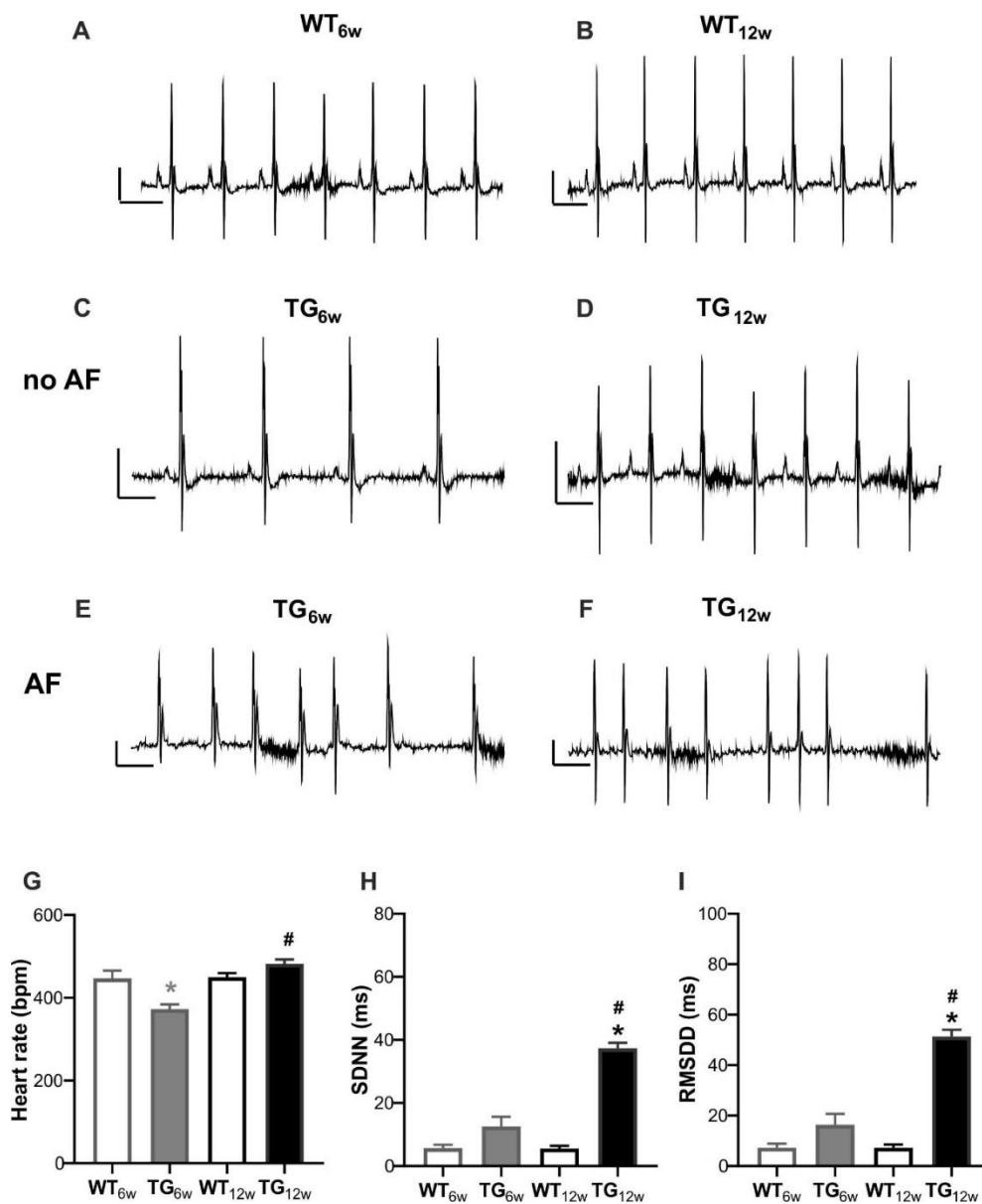
Left atria of all 4 experimental groups of mice were dissected in oxygenated ice cold physiological solution and attached to a force transducer for recording isometric contractions electrically driven by field stimulation at 1 Hz using suprathreshold rectangular pulses of 5 ms duration, as described previously²⁷. Before the experimental protocol, atria were pre-stretched with a force of 5 mN and were allowed to equilibrate at 37°C for at least 30 minutes in a bath solution containing (in mM): 120 NaCl, 5.4 KCl, 1.8 CaCl₂, 1 MgCl₂, 22.6 NaHCO₃, 0.42 NaH₂PO₄, 0.28 ascorbic acid, 0.05 Na₂EDTA and 5.5 glucose, adjusted to pH 7.4 with NaOH. To build the dose-response curves, the concentrations of carbachol (CCh) or isoproterenol (ISO) were increased every 5 minutes to the following concentrations (in M): 10⁻⁹, 10⁻⁸, 3x10⁻⁸.

⁸, 10^{-7} , 3×10^{-7} , 10^{-6} , 10^{-5} and 10^{-4} M, while the force of contraction was monitored continuously. Dose response curves were built using the force of contraction measured for each drug concentration at steady state. Six out of 12 WT_{6w} and 10 out of 24 WT_{12w} atria did not show a positive staircase in response to ISO application after CCh, therefore these results were excluded from the calculation of half-maximal effective concentration (EC₅₀).

Statistics

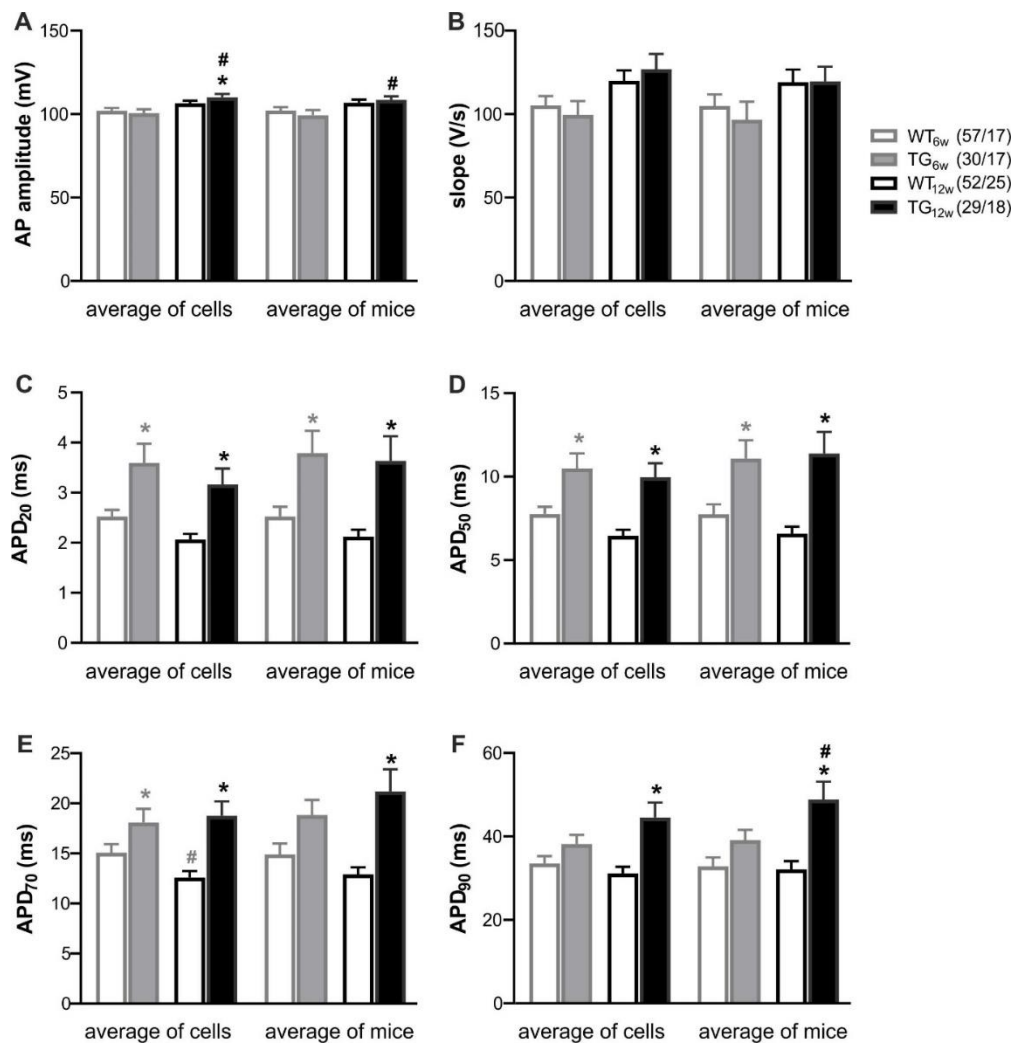
Data are reported as mean values \pm standard error (SE) with n indicating the number of cells and N the number of animals. Normal distribution was assessed using Shapiro-Wilk test in GraphPad 8.0 (GraphPad Software, La Jolla, California, USA). According to the Gaussian distribution, student's *t* test or Mann-Whitney test or Wilcoxon matched-pairs signed rank test were used for two group comparison, and one-way ANOVA test with Newman-Keuls post-hoc test or Kruskal-Wallis test with Dunn's post-hoc test were used for multiple groups comparison. Current-voltage relations and dose-response curves were compared using 2-way repeated measures ANOVA with Bonferroni post-hoc test. Relative gene expression ratios were expressed as mean values \pm standard error (SE) for qRT-PCR and ChIP experiments as reported by the relative expression software tool (REST_v, (version 2.07)²⁴. Data were considered significantly different at $P < 0.05$.

Figure S1. *In vivo* electrophysiology of CREM TG mice.



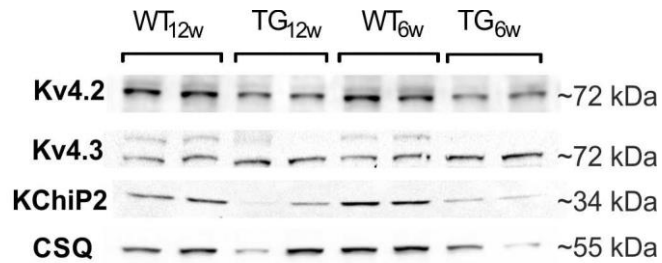
(A-F) Representative electrocardiograms (ECG) recorded from wildtype mice young (6 weeks, WT_{6w}, **A**) and older (12 weeks, WT_{12w}, **B**) and from CREM transgenic (TG) mice young (TG_{6w}, **C**, **E**) and older (TG_{12w}, **D** and **F**) showing no AF (**C**, **D**) and AF (**E**, **F**). Scale bars: vertical 0.2 mV, horizontal 0.1 s. (**G-I**) Analysis of ECG parameters of heart rate variability (HRV): mean heart rate (**G**), standard deviation of NN intervals (SDNN, **H**), root mean square of the successive differences between neighboring RR intervals (RMSDD, **I**). Data show mean \pm SE resulted from 12 (WT_{6w}), 36 (TG_{6w}), 34 (WT_{12w}) and 54 (TG_{12w}) ECG traces. * $P < 0.05$ for TG_{6w} vs. WT_{6w} (grey), TG_{12w} vs. WT_{12w} (black), # $P < 0.05$ TG_{12w} vs. TG_{6w} (black) from parametric or non-parametric 1-way ANOVA with the corresponding post-hoc test.

Figure S2. Basal properties of the action potentials (AP) of atrial myocytes isolated from CREM TG mice.



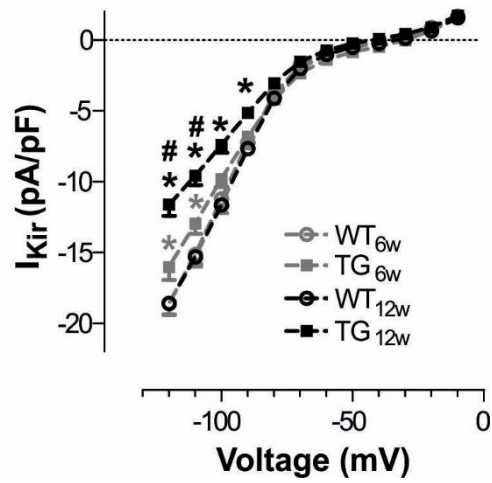
AP parameters such as AP amplitude (A), slope of depolarization (B), and AP duration (APD) from peak to 20, 50, 70 and 90% repolarization (C-F) were measured in the 4 groups of animals. Data show mean \pm SE of the values of parameters calculated for individual cells of the group (average of cells) or the mean value of the averaged parameter calculated per heart (average of mice). In the legend, the numbers in brackets show number of cells / number of mice. * $P < 0.05$ for TG_{6w} vs. WT_{6w} (grey), TG_{12w} vs. WT_{12w} (black), # $P < 0.05$ WT_{12w} vs. WT_{6w} (grey), TG_{12w} vs. TG_{6w} (black) from parametric or non-parametric 1-way ANOVA with the corresponding post-hoc test.

Figure S3. Representative uncut immunoblots presented in Fig.2, showing the transient outward channel components: the forming α -subunits Kv4.2, Kv4.3 and auxiliary subunit KChIP2, vs. the myocyte marker calsequestrin (CSQ) used for normalization.



Two samples of each group have been loaded on the gel, as mentioned above the immunoblots. Number on the right represent the relative size of the proteins.

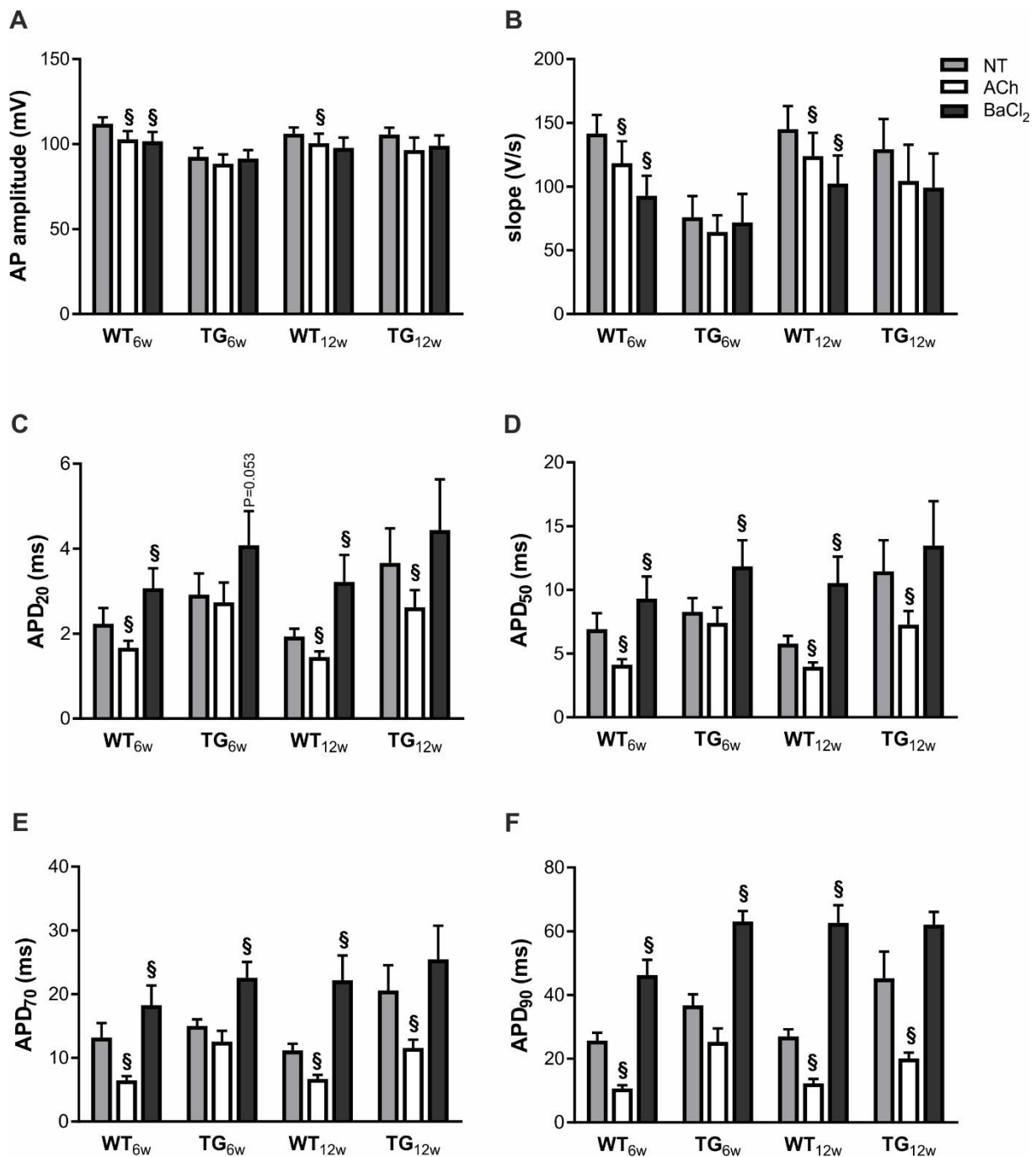
Figure S4. Total inward K^+ -current of TG atrial myocytes, before and after AF onset.



Data show mean \pm SE of averaged I-V plots of the current density at the end of the hyperpolarizing pulse (I_{Kir}), recorded from the four experimental groups. n/N = 33–55/11–18.

* $P < 0.05$ for TG_{6w} vs. WT_{6w} (grey), TG_{12w} vs. WT_{12w} (black), # $P < 0.05$ TG_{12w} vs. TG_{6w} (black) from 2-way repeated measures ANOVA with Bonferroni post-hoc test.

Figure S5. Action potential (AP) parameters following blocking or activating I_{K1} and I_{KACH} , respectively, of atrial myocytes isolated from CREM TG mice.



Data show mean \pm SE of AP amplitude (A), slope of depolarization (B), and AP duration (APD) from peak to 20, 50, 70 and 90% repolarization (C-F) measured in the 4 groups of animals. n/N for WT_{6w} (7/5) TG_{6w} (5/5), WT_{12w} (11/6) and TG_{12w} (5/4). $^{\$}P < 0.05$ BaCl₂ or ACh vs. normal Tyrode (NT) using Wilcoxon matched pairs signed rank test.